

1 **A review of undulated sediment features on**
2 **Mediterranean prodeltas: distinguishing sediment**
3 **transport structures from sediment deformation**

4
5 *Roger Urgeles¹, Antonio Cattaneo², Pere Puig¹, Camino Liqueste³, Ben De Mol^{4,5}, Nabil*
6 *Sultan², Fabio Trincardi⁶*

7
8 ¹*Dept. Geologia Marina, Institut de Ciències del Mar (CSIC), Pg. Marítim de la*
9 *Barceloneta, 37-49, 08003 Barcelona, Catalonia, Spain*

10 ²*IFREMER, GM-LES, F-29280 Plouzané Cédex, Bretagne, France*

11 ³*European Commission - Joint Research Centre, Institute for Environment and*
12 *Sustainability, Rural, Water and Ecosystem Resources Unit, Via E. Fermi 2749,*
13 *TP 460, 21027 Ispra (VA), Italy*

14 ⁴*Dept. Estratigrafia, Paleontologia i Geociències Marines, Facultat de Geologia, c/*
15 *Martí i Franquès s/n, 08028 Barcelona, Catalonia, Spain*

16 ⁵*Parc Científic de Barcelona, c/ Adolf Florensa 8, 08028 Barcelona, Catalonia, Spain*

17 ⁶*ISMAR (CNR), v. Gobetti 101, 40129 Bologna, Italy*

18 **Abstract**

19 Most Mediterranean prodeltas show undulated sediment features on the foresets of their
20 Holocene wedges. These features have been described all along the Mediterranean for
21 the last 30 years and interpreted as either soft sediment deformation and incipient
22 landsliding, and more recently, as sediment transport structures. We perform a review
23 and detailed analysis of these undulated sediment features using ultrahigh-resolution
24 seismic and bathymetric data as well as geotechnical information and hydrodynamic
25 time series and hydrographic transects. In this study we show that the characteristics of
26 the sediment undulations (configuration of the reflections down section and between
27 adjacent undulations and overall morphologic characteristics) are incompatible with a
28 genesis by sediment deformation alone and do not show evidence of sediment
29 deformation in most cases. Various processes in the benthic boundary layer can be
30 invoked to explain the variety of features observed in the numerous areas displaying
31 sediment undulations.

32

33 **Keywords**

34 Undulated sediments, prodeltas, slope failure, sediment waves, hyperpycnal flows,
35 internal waves

36 **Introduction**

37 The last two decades have provided profuse evidence of undulated sediment features on
38 Mediterranean prodeltas (Galignani, 1982; Mougnot et al., 1983; Aksu and Piper,
39 1988; Checa et al., 1988; Trincardi and Normark, 1988; Romagnoli and Gabbianelli,
40 1990; Agate and Lucido, 1995; Ercilla et al., 1995; Chiocci et al., 1996; Correggiari et
41 al., 2001; Lykousis et al., 2001; Marsset et al., 2004; Cattaneo et al., 2004; Fernandez-
42 Salas et al., 2007; Urgeles et al., 2007; Lykousis et al., 2008; Agate et al., 2009;
43 Rebesco et al., 2009; Bárcenas et al., 2009)). Early studies on these features proposed
44 interpretations involving sediment deformation and slope failure phenomena (Galignani,
45 1982; Mougnot et al., 1983; Aksu and Piper, 1988; Checa et al., 1988; Romagnoli and
46 Gabbianelli, 1990; Agate and Lucido, 1995; Ercilla et al., 1995; Chiocci et al., 1996;
47 Correggiari et al., 2001; Lykousis et al., 2001; Fig. 1). Such evidences came from
48 seismic reflection profiles where sediment undulations appeared to be separated by
49 shear planes.

50 With popularization of very high resolution chirp-sonar profiling and mapping systems
51 based on multibeam technology, seafloor surface geometries compatible with submarine
52 slope deformation alone were questioned (Cattaneo et al., 2004; Urgeles et al., 2007;
53 Fernandez-Salas et al., 2007; Bárcenas et al., 2009). An intense debate started on
54 whether these features were in fact created by sediment transport processes on the
55 bottom boundary layer (i.e. we were imaging sediment waves), or by deformation.
56 Mixed theories (i.e. initial sediment deformation and growth by differential sediment
57 accumulation patterns) were also proposed (Cattaneo et al., 2004). The resolution of the
58 geophysical data used to investigate those features appeared not high enough or not
59 comparable to the outcrop scale analogs, where soft sediment deformation structures
60 can be readily identified on paleo-prodeltas (Bhattacharya and Davies, 2001), to be able
61 to assign a genetic mechanism to these structures. The debate was not restricted to the
62 Mediterranean Sea, a few specific case studies in shallow water settings (Bornhold and
63 Prior, 1990; Mosher and Thompson, 2002; Boe et al., 2004; Hill et al., 2008) and deep-
64 water settings (Field and Barber, 1993; Gardner et al., 1999; Lee et al., 2002) of various

65 areas of the world ocean also attracted quite vivid debate (e.g. the Humboldt slide off
66 northern California; [Normark et al., 1979](#); [Normark, 1980](#); [Gardner et al., 1999](#)).
67 Significant efforts have been carried out to understand undulated sediment features in
68 deep-water settings, which has been shown that a variety of process are also able to
69 shape undulated sediment features in these environments ([Wynn and Stow, 2002](#)),
70 though deep-water undulations are at least one order of magnitude larger ([Nakajima and](#)
71 [Sato, 2001](#)).

72 In the case of Mediterranean prodeltas, with one of the most heavily populated
73 coastlines of the world, the identification of the sediment undulations as depositional or
74 deformation features has important implications for offshore and coastal management
75 ([Trincardi et al., 2004](#); [Urgeles et al., 2007](#)). This triggered a multidisciplinary
76 investigation that included collection of oceanographic and geotechnical data. Efforts
77 were put to model and monitor active sediment transport on the seafloor ([Puig et al.,](#)
78 [2007](#); [Sultan et al., 2008](#)). The aim of this paper is to provide new data and the latest
79 view on the origin of these undulated seafloor features in the prodeltas of the
80 Mediterranean Sea, where this type of structures share many characteristics that are not
81 found in deeper water settings.

82

83 Mediterranean setting

84 The Mediterranean region is seismically active, and is currently undergoing rather rapid
85 deformation ([Vannucci et al., 2004](#); [Jiménez-Munt et al., 2006](#)). In a very simplified
86 way, the Mediterranean region records, from west to east, a passage from a simple
87 deformation at the oceanic plate boundaries of the Atlantic, characterized by narrow
88 seismic belts, to a broad belt of seismicity and deformation that characterizes the
89 continental collision setting ([McKenzie, 1972](#); [England and Jackson, 1989](#)). Seismicity
90 is widespread in the Mediterranean region, although it is not restricted to narrow
91 seismogenic boundaries, but is generally rather diffuse. The eastern Mediterranean and
92 the Aegean Sea in particular, are the most active seismic regions.

93 The system of extensional Mediterranean basins have been formed during the latest
94 phases of subduction of several segments of the Tethys oceanic lithosphere and the
95 extensional orogenic collapse caused either by delamination of thickened continental
96 lithosphere ([Platt and Vissers, 1989](#); [Docherty and Banda, 1995](#); [Vissers et al., 1995](#);
97 [Seber et al., 1996](#); [Platt et al., 1998](#); [Calvert et al., 2000](#)), rollback of oceanic plates

98 (Lonergan and White, 1997), or a combination of both processes (Faccenna et al.,
99 2004). Subduction is also responsible for the formation of contractional belts like the
100 Apennines or the Betics. Typically those belts have also undergone extensional
101 processes, which in a number of cases are currently active, as is the case in the Betics
102 (Balanyá et al., 1997; Johnson et al., 1997; Martínez-Martínez y Azañón, 1997) and in
103 the Apennines (Collettini, 2004, 2005). The coastal morphology of the Mediterranean
104 Sea is a direct result of the tectonic setting and it is characterized by coastal mountain
105 ranges with high mountain peaks in the catchment basins of the rivers and areas of
106 tectonic uplift.

107 Mediterranean climate and sediment delivery to Mediterranean prodeltas

108 The Mediterranean climate shows a marked seasonal regime modified locally by
109 complex geographic factors. During the long summer season the subtropical circulation
110 causes warmth and dryness, while in winter the temperate circulation brings milder and
111 wetter air masses from the north-east. The Mediterranean Sea has a role of heat
112 reservoir and source of moisture for surrounding land areas. The Mediterranean climate
113 is also characterized by the presence of regional energetic mesoscale features and
114 cyclogenesis areas (Lionello et al., 2006).

115 Most of the Mediterranean drainage network is made of medium-to-small fluvial
116 systems, with only 9 rivers longer than 450 km (Nile, Ebro, Rhone, Chelif, Po,
117 Moulouya, Ceyhan, Evros and Medjerda; Fig. 1). The Mediterranean river systems
118 show relatively high temperature, small size, high seasonal variability, high population
119 density, and high slope due to the short distance between the mountain ranges and the
120 coast (Liquete et al., in prep.). In general, rivers from the northern Mediterranean region
121 are orographically more abrupt, climatically colder and wetter, and hydrologically more
122 active. The largest runoff ($>1000 \text{ mm}\cdot\text{yr}^{-1}$) is found in a few Greek and Albanese rivers
123 associated with the greatest precipitation falls over the Albanian and Croatian basins.
124 Italy concentrates the watersheds with more erodable and less vegetated land. The most
125 arid conditions are typically found in North African, Sicilian and Spanish Levantine
126 river basins.

127 The current freshwater surface discharge to the Mediterranean Sea is estimated in 400-
128 $450 \text{ km}^3\cdot\text{yr}^{-1}$, about one half of what it was at the beginning of the 20th century (UNEP,
129 2003; Ludwig et al., 2009). It is suggested that the overall sediment flux to the
130 Mediterranean Sea is $730 \times 10^6 \text{ t}\cdot\text{yr}^{-1}$ (UNEP, 2003).

131 Available measurements from 88 Mediterranean watersheds (Milliman and Syvitski,
132 1992; Probst and Amiotte-Suchet, 1992; UNEP, 2003; RIKZ et al., 2004; EEA, 2006;
133 FAO, 2007; Syvitski and Milliman, 2007; Liqueste et al., 2009) allowed estimating their
134 average suspended sediment yield in $352 \text{ t}\cdot\text{km}^{-2}\cdot\text{yr}^{-1}$, which is approximately twice the
135 $150\text{-}200 \text{ t}\cdot\text{km}^{-2}\cdot\text{yr}^{-1}$ world average (Milliman and Syvitski, 1992). The relatively low
136 water discharge of these systems (see for instance FAO, 2007) related to their moderate-
137 to-high sediment flux suggests that the Mediterranean watersheds are particularly
138 competent as sediment suppliers to the sea. The lowest sediment discharge values are
139 found in the NW Mediterranean region, notably in France and Spain (UNEP, 2003;
140 EEA, 2006; Liqueste et al., 2009), although the fluvial sediment load is known to be
141 highly variable in the area.

142 Mediterranean wave and tidal regime

143 The Mediterranean Sea has a relatively mild climate on the average, but substantial
144 storms are possible, usually in winter. The maximum measured significant wave height
145 reaches 10 m, but model estimates for some non-documented storms suggest much
146 larger values (Cavalieri et al., 2005). The winter mean significant wave height in the
147 Mediterranean ranges from ~ 0.8 to ~ 2 m. The area with the largest winter mean
148 significant wave height is the Gulf of Lions, in the Western Mediterranean Sea
149 (Cavalieri et al., 2005). Wave dynamics in the Mediterranean Sea is mostly influenced
150 by the regional orographic conformation and fetch (Lionelli and Sanna, 2005).

151 Tidal currents in the Mediterranean Sea are important only close to major passages (e.g.
152 the Strait of Gibraltar, the Channel of Sicily), in some minor ones (e.g. the Strait of
153 Messina) as well as in all coastal pond outlets where they can reach a few m s^{-1} (Millot
154 and Taupier-Letage, 2005b). Over most of the Mediterranean, however, tidal currents
155 can be neglected since they have a velocity of a few mm s^{-1} only (Alb erola et al., 1995).
156 Also tidal amplitude rarely exceeds 0.5 m except in the Gulf of Gabes off the coast of
157 Tunisia (tide range of nearly two meters) and areas where amplification occurs due to
158 summing of the coastal setup and seiches, as in the northern Adriatic (Tsimplis et al.,
159 1995).

160 Oceanography of shallow Mediterranean waters

161 The semi-enclosed Mediterranean Sea is characterized by evaporation exceeding
162 precipitation and river runoff (Le Vouch et al., 1992; Millot and Taupier-Letage,

163 2005a). The tendency for a difference in level between the sea and the Atlantic Ocean
164 leads the surface Atlantic Water to flow into the Mediterranean Sea (Millot and
165 Taupier-Letage, 2005b). The incoming Atlantic Water is continuously modified due to
166 interactions with the atmosphere and mixing with older Atlantic Water remaining at the
167 surface and with the waters underneath (Fig. 1).

168 In winter, cold and dry air masses entrained by relatively brief episodes of strong
169 northerly winds induce marked evaporation and direct cooling of modified Atlantic
170 Water, resulting in a dramatic increase in its density which makes it sink. Sinking and
171 deep-water formation occurs in a series of specific zones where deep dense water
172 convection takes place, generally located in the northern parts of the basins (Fig. 1).
173 Due to the Coriolis Effect all waters that are forced to circulate at basin scale (at all
174 depths) tend to follow, in the counterclockwise sense, the isobaths corresponding to
175 their density level (Millot and Taupier-Letage, 2005b). Several evidences show that
176 current circulation could be associated with bedforms at several deep-water sites of the
177 Mediterranean, including the Sicily Channel, the Southern Adriatic Margin and the
178 Corsica Basin (Verdicchio and Trincardi, 2009).

179 On the continental shelves of the northern Mediterranean basins (i.e. Gulf of Lions,
180 northern Adriatic and northern Aegean), waters are markedly cooled during wintertime
181 because the reduced depth does not represent a large reservoir of heat. Despite the gain
182 in buoyancy caused by freshwater inputs due to river runoff, dense waters are also
183 generated on the northern Mediterranean shelves. Such dense waters travel along the
184 shelf and cascade to greater depths, mainly through submarine canyons, until reaching
185 their density equilibrium level (Durrieu de Madron et al., 2005). These waters are
186 rapidly lost due to mixing induced by the relatively intense circulation along the slope
187 (Le Vouch et al., 1992).

188 Sea level history in the Mediterranean Sea

189 The Quaternary is characterized by cyclic climate and related sea-level changes
190 (Shackleton, 1987) that strongly impacted the sedimentary architecture of continental
191 margins. These events have also strongly influenced sediment distribution and
192 architecture of sedimentary bodies in continental shelves of the Mediterranean Sea (e.g.
193 Jouet et al., 2006; Berne et al., 2007; Cattaneo et al., 2007; Lique et al., 2007). The
194 Quaternary climate changes also had a profound effect on adjacent river watersheds,

195 which resulted in a sedimentary flux 3 to 3.5 times greater than the present one, during
196 the maximum of glaciation (Bossuet et al., 1996).

197 During the last glacial-interglacial cycle, the Mediterranean Sea has been connected to
198 the global ocean and therefore has followed the same trends in sea-level changes (Berné
199 et al., 2007). Isotopically-derived sea-level curves for the last 120 kyr (e.g. Shackleton,
200 2000, Waelbroeck et al., 2002) display a general fall until the LGM, punctuated by
201 high-frequency changes. The last sea-level lowstand is generally set around 110 and 120
202 m below present sea-level, but estimates going from 90 to 150 m have also been
203 proposed (Shackleton, 1977, Fairbanks, 1989, Bard et al., 1990, Lambeck and Bard,
204 2000 and Clark and Mix, 2002). The position of relative sea-level during the maximum
205 lowstand is at least 115 m in the Mediterranean Sea (Jouet et al., 2006).

206 On Mediterranean continental shelves, sediment supply decreased abruptly at 15 kyr
207 BP, because of the rapid landward shift of fluvial outlets during the deglacial sea-level
208 rise (e.g. Jouet et al., 2006). Sea-level rise for the Post Younger Dryas period in the
209 Mediterranean show a constant global sea-level rise with values between 1 and 1.5
210 cm/yr (Lambeck and Bard, 2000; Berné et al., 2007). Archaeological observations along
211 the Mediterranean coast indicate that sea level remained below its present level until
212 about 3 ka BP (Lambeck et al., 2004). High frequency sea-level fluctuations during the
213 last 4 ky were relatively minor, fluctuating by less than 1 m (Lambeck and Bard, 2000;
214 Sivan et al., 2001). Hernández-Molina et al. (1994) also show that during Late
215 Pleistocene-Holocene times, climate-induced relative changes in sea level were faster
216 than fault movements or local subsidence, at least on the Iberian Mediterranean coast.

217 **Methods**

218 The evidences discussed in this manuscript are mainly based on a set of previously
219 published data. Published data were obtained using a variety of tools with differing
220 resolution, penetrations, spatial and temporal coverage. They include shallow water
221 multibeam echosounder (Cattaneo et al., 2004; 2006; Urgeles et al., 2007; Fernández-
222 Salas et al., 2007; Rebesco et al., 2009), seismic reflection profiles (Aksu and Piper,
223 1988; Checa et al., 1988; Mougnot et al., 1983; Trincardi and Normark, 1988; Díaz
224 and Ercilla, 1993; Ercilla et al., 1995; Chiocci et al., 1996; Cattaneo et al., 2004; 2006;
225 Urgeles et al., 2007; Fernández-Salas et al., 2007; Lykousis et al., 2008; Rebesco et al.,
226 2009; Agtate et al., 2009), high resolution 3D seismic data (Marsset et al., 2004),
227 hydrodynamic time series and hydrographic transects across undulated seafloor features

228 (Puig et al., 2007), sediment samples for geotechnical tests (Sultan et al., 2004; 2008),
229 CPT insitu measurements (Sultan et al., 2004; 2008) and river water and sediment
230 discharge obtained from several regional and global databases (Liquete et al., in prep.).
231 For the details on these data sets the reader is referred to the original sources where these
232 data were published.

233 Unpublished data presented in this paper, shedding additional light into the processes at
234 the origin of these undulations, include ultra-high resolution chirp profiles from the
235 Adriatic, Algerian and Llobregat areas. The systems used in these areas are respectively
236 the CHIRP sonar of the R/V Urania, the 2.5-5.5 kHz hull-mounted source of the R/V
237 L'Atalante operated with the 'CHEOPS' acquisition software, and a Simrad TOPAS
238 PS-040 5 kHz parametric echosounder,. We also show bathymetric data from the central
239 Adriatic obtained with an EM300 Simrad multibeam echosounder operated from the
240 vessel Odin Finder (see details in Cattaneo et al., 2004), and Simrad EM3000 data off
241 the eastern Iberian prodeltas. The sediment core data off Bourmedes was acquired from
242 the R/V L'Atalante through a Kullenberg piston core.

243 These high-resolution data are a key to identify the origin of the sediment undulations,
244 as they provide details that were unadverted in previous lower resolution surveys.

245 **Morphology**

246 Most sediment undulations in Mediterranean prodeltas develop in water depths ranging
247 between 20 and 100 m, mainly beyond the clinoform rollover point, on the steepest part
248 of Holocene prodeltas. They are found on slopes between 0.2° and 3° (average 2°) and
249 affect areas of different size (3.7 km² in the Ebro prodelta, 25 km² in the Llobregat
250 prodelta, 25.7km² on the Guadalfeo, 100 km² in the Tiber prodelta and about 800 km²
251 on the central Adriatic shelf). They commonly present a relatively elongated shape
252 controlled by the two isobaths mentioned above (Fig. 2A). In cross-section the area
253 where the undulations develop is commonly concave upward. Where multibeam data is
254 available the undulation crests are more or less parallel to the bathymetric contours and
255 have slightly sinuous to rectilinear shape in planform view (Cattaneo et al, 2004;
256 Fernandez-Salas et al., 2007; Urgeles et al., 2007; Fig. 2, 3). Exceptions to this occur in
257 the Ebro and Fluvià-Muga prodeltas where the sediment undulations have crests
258 respectively perpendicular and oblique to the bathymetric contours and develop within
259 shallower or deeper depth ranges (8-15 m and 60-100 m respectively; Table 1 and Fig.
260 2C). The undulations often show an intricate pattern of bifurcating and truncated ridges

261 and can be traced for distances ranging between a few tens of meters to 2 km, but most
262 commonly range in between 200 to 400 m.

263 The amplitude and wavelength (see also Cattaneo et al., 2004) of the sediment
264 undulations is variable. From crest to trough the undulations range from as high as 5 m
265 to a few cm (Table 1; Fig. 4). They also range from about 300 m wavelength to about
266 20 m in sediment undulations that develop in relatively shallow waters and those that
267 extend from shallow to deeper waters in the prodelta foresets. However, undulations
268 that develop only in the deeper parts of the prodelta show larger wavelengths that may
269 reach up to 1 km (Fig. 4). Generally no trend is observed in wave amplitude or wave
270 length with water depth and increasing distance from shore. This is specially the case
271 for the deeper prodeltaic undulations. However, where undulations develop over
272 extensive areas and are better developed, such as in the Adriatic (Cattaneo et al., 2004)
273 and in the Llobregat prodelta (Urgeles et al., 2007), the undulations tend to show a
274 decrease both in wavelength and amplitude with water depth, especially for those
275 situated above 40 mwd. The shallower undulations show relatively short upslope limbs
276 and long downslope limbs (near 0 asymmetry values) while in deeper waters the
277 undulations are more symmetric. In the Adriatic Sea these undulations are associated in
278 some cases with small-scale mud reliefs in water depths of 70 to 110 m, with preferred
279 crest orientations that are perpendicular to regional contours (Marsset et al., 2004). The
280 association of these two features is continuous along some kilometers to tens of
281 kilometers in three sectors of the central Adriatic shelf, but it is not ubiquitous (Fig. 5).
282 The undulations that develop on the prodeltas of the Mediterranean Sea generally have
283 L/H ratios in the range of 50-400 (Fig. 4). The wavelength is on the tenths to hundreds
284 of meters scale. This contrasts with deep-water sediment waves that have wavelengths
285 in the km scale (Wynn and Stow, 2002). Similarly sediment undulations on prodelta
286 wedges of the Mediterranean Sea are only a few meters high, while deep-water
287 sediment waves worldwide are tens of meters high (Wynn and Stow, 2002). Within the
288 sediment undulations that develop on the continental shelves of the Mediterranean,
289 those that are attached to the inner shelf have generally shorter wavelengths, than those
290 that occur on the mid-shelf (e.g. Fluvià-Muga; Fig. 2c and Table 1).

291 **Seismostratigraphic analysis**

292 On the new and published seismic reflection profiles, the sediment undulations of
293 Mediterranean prodeltas hold the following common characteristics: 1) They are rooted

294 at the Maximum Flooding Surface (MFS) or a secondary flooding surface and develop
295 on the Late-Holocene High-stand Systems Tract (HST) mud wedge (Figs. 3, 6 and 7);
296 2) the shallowest parts of these undulated prodeltas appear largely void of reflectors or
297 these appear with a very low amplitude and more chaotic character (see [Trincardi and](#)
298 [Normark, 1988](#); [Correggiari et al., 2001](#); [Cattaneo et al., 2004](#); [Urgeles et al., 2007](#);
299 [Lykousis et al., 2009](#)). This facies is distinctive of shallow gas enriched sediment layers,
300 which mask the underlying reflectors (Sultan et al., 2008); 3) in most cases, sediment
301 undulations develop downslope from the gas front, and only at a few locations the
302 uppermost undulations are on top of the gassy zone (e.g. the Ebro prodelta); 4) the
303 sediment undulations are mostly characterized by a uniform wavy stratified pattern of
304 strong to faint prograding seismic reflectors on the prodelta front, in which both
305 wavelength and amplitude of the undulations generally decrease with increasing
306 stratigraphic depth (Figs. 6, 7 and 8).. Where this seismic character is present (most
307 prodelta settings except the prodeltas of Andalusia) the sediments are probably quite
308 homogeneous and fine grained (see Table 1). Borehole samples confirm that the
309 sediment composition of the undulations is quite homogeneous ([Cattaneo et al., 2003](#)).
310 Where piston cores are available, the dominant lithology is muddy, as in the case of the
311 the Algerian shelf (Fig. 8) and central Adriatic ([Cattaneo et al., 2004](#); [Sultan et al.,](#)
312 [2008](#), Fig. 9). The prodeltaic Holocene mud wedges that are affected by the undulations
313 have thicknesses that do not exceed 50 ms TWTT and extend offshore for a few
314 kilometers (generally <10 km).

315 The analysis of high resolution seismic reflection profiles shows that undulations at the
316 seafloor may correspond to more than one undulation below seafloor and the opposite
317 way-round: various undulations on the seafloor may correspond to one single
318 undulation below seafloor (Figs. 6-8). Also areas that do not presently show undulations
319 at the seafloor, may show evidences of seafloor undulations down section, with the
320 undulations being truncated at the seafloor (Fig. 6 and 8). This pattern occurs in the
321 shallowest water depths. At other locations where the seafloor is devoid of undulations
322 but sediment undulations are present on the stratigraphic record, the undulations are
323 masked by more recent sedimentation concealing the undulations (Fig. 8). These two
324 examples of undulation suppression indicate that, within late Holocene prodeltas,
325 differential deposition or erosion may smoothen out pre-existing seafloor undulations.

326 The crest and trough angle of climb of most sediment undulations are not homogeneous
327 down section (Fig. 6 and 8). Variations are also not consistent, i.e. the angle may

328 increase or decrease or change in trend down section, i.e. displaying alternations
329 between convex and concave shapes (Fig. 6).

330 The largest sediment undulation fields in the Adriatic and Llobregat prodeltas are
331 predominantly muddy (respective average clay, silt and sand contents of 65%, 35% and
332 5% in the Adriatic and 15%, 46% and 39% in the Llobregat). In relatively energetic
333 environments like the “Ramblas” in southern Andalusia, (Bárcenas et al., 2009) the
334 sediment undulations may be formed by coarser material, being sand the predominant
335 grain size fraction (Table 1).

336 **Geotechnical investigations**

337 Samples for deep geotechnical investigation have only been obtained in the Adriatic Sea
338 where a major European effort (project PROMESS-1) aimed to understand the genesis
339 of these undulations through drilling (Sultan et al., 2008). Shallow geotechnical data
340 exists also for other areas such as the Tiber pordelta (Tommasi et al., 1998). The drilling
341 in the Adriatic Sea was targeted to penetrate through one of the potential shear planes in
342 between two sets of undulation packages and through the MFS. This area is particularly
343 active in terms of earthquakes and there was a concern that seismic ground motions
344 where at the origin of the observed seafloor undulations. Undrained shear strength data
345 measured with a hand operated torvane shortly after the cores were acquired, an
346 automated laboratory shear vane and laboratory fall cone showed quite consistent
347 results, indicating that a sharp increase in shear strength of about 12 kPa occurred when
348 moving from the upper to the lower undulation (Fig. 9). Cyclic triaxial tests indicated
349 that silty and sandy sediments such as those occurring near the MFS (Fig. 9) were the
350 most sensitive to earthquake loading. Pre-consolidation pressures measured with an
351 incremental loading oedometer indicated normal to slightly underconsolidated
352 sediments in the upper undulation and a higher degree of underconsolidation within the
353 undulation directly below the plane separating the two undulations (Fig. 9). However, it
354 was found that neither sediment accumulation rates nor earthquake ground motions
355 could explain the excess pore pressure resulting from this consolidation state (Sultan et
356 al., 2004; 2008). It was suggested that overpressure could result from gas generation
357 (Sultan et al., 2008). The facts above were not incompatible with an origin by sediment
358 deformation. To the contrary, such a situation would be favorable to deformation by
359 earthquake shaking. Therefore, an analysis of the slope stability under cyclic ground
360 motions due to earthquakes was undertaken having into account historical earthquake

361 records and in situ ground shaking measurements performed with Ocean Bottom
362 Seismometers (Sultan et al., 2008). Assessment of the sediment liquefaction potential
363 was made using Cyclic1D, a nonlinear finite element program for execution of one-
364 dimensional site amplification and liquefaction (Elgamal et al., 2002). The simulation
365 showed that, for characteristic earthquakes in that area, liquefaction of the level above
366 which the undulations detach and deformation of the overlying sediment, could only
367 occur when that level was only 5 mbsf or shallower. It was shown that further burial and
368 increase in confining lithostatic pressure actually prevents sediment liquefaction (Sultan
369 et al., 2008).

370 **Sediment transport processes**

371 The sedimentary dynamics in the Mediterranean continental shelves has been
372 continuously studied during the last decades in the framework of many research
373 projects. However, few studies have been conducted in prodeltaic areas affected by
374 undulated seafloor features using bottom boundary layer instrumentation (e.g.
375 Cacchione et al., 1990; Jiménez et al., 1999; Puig et al. 2001; Palanques et al., 2002;
376 Fain et al., 2007); and to our knowledge, only one of them (Puig et al., 2007) was
377 addressed to establish relationships between active sediment dynamics and the
378 formation/maintenance of the undulated seafloor features. This study was conducted in
379 the western Adriatic, off Pescara (Fig. 10), in a region characterized to have large
380 portions of the late Holocene prograding mud wedge affected by seafloor undulations.

381 The proposed observational approach consisted in measuring sediment transport process
382 across an undulated cliniform by means of deployments of two boundary-layer tripods
383 in 12 and 20 m water depth and a mooring in 50 m water depth, right in the middle of
384 the undulations. This mooring line was equipped with two RCM-9 current meters
385 placed at 2 meters above the seafloor (masf) and at 20 m water depth, in intermediate
386 waters 30 masf. Thermistors were also mounted on the mooring line at numerous
387 heights above the seabed between the two current meters. Observations took place from
388 late October 02 to early May 03 in two consecutive three-month deployments and
389 hydrographic sections were conducted at the time of instruments deployment,
390 maintenance and retrieval (see Puig et al., 2007 for details).

391 The across-shelf distributions of temperature, salinity and suspended sediment
392 concentration (SSC) in the study area during November 2002 are shown in Fig. 10.
393 Temperature and salinity hydrographic transects clearly reflected the presence of coastal

394 waters influenced by the discharges from the Po and Apennine rivers, which occupied
395 the entire topset region and were characterized by having lower salinities and colder
396 temperatures than the offshore waters. Water temperature distribution in November
397 2002 also reflected the typical late-summer situation for Mediterranean surface waters,
398 showing a wide and well-developed thermocline with the maximum gradient between
399 40 and 80 m water depth, coinciding with the region affected by the undulated seafloor
400 (Fig. 10). SSC distribution indicated the presence of a surface nepheloid layer, being
401 constrained by coastal colder and less saline waters, and the development of a bottom
402 nepheloid layer that detaches where the thermocline intersected with the seabed (Fig.
403 10A).

404 Sediment transport processes were analyzed at the topset and foreset region of the
405 undulated clinoform and the role of wave-current interaction and internal waves on
406 sediment resuspension were investigated. Several sediment-resuspension events were
407 recorded at the tripod site, mainly related to Bora and Sirocco storms, during which
408 current and wave shear stresses reached similar values. After the passage of a storm,
409 activity of near-inertial internal waves (~17 h) was also recorded by the moored current
410 meters and temperature sensors (Fig. 10B).

411 During periods characterized by strong near-inertial fluctuations, increases of the water
412 SSC clearly coincided with the offshore direction of the cross-shelf velocity component
413 and with strong temperature and salinity fluctuations showing excursions through the
414 water column of tens of meters (Fig. 10B). During the sediment transport events
415 associated to the passage of internal waves, current directions are aligned normal to the
416 crests of the seafloor undulations, exporting suspended sediment in an oscillatory way
417 from the topset to the bottomset region of the clinoform.

418 **Discussion: Origin of the sediment undulations: sediment deformation or** 419 **bedforms formed by bottom boundary layer processes**

420 The characteristics of individual sediment undulations and that of the sediment
421 undulation field sometime provide inconclusive evidence of the process at the origin of
422 such morphology. For instance, most sediment undulation fields like the Llobregat or
423 central Adriatic have a shape elongated along the direction of the prevailing bottom
424 currents (parallel to the bathymetric contours), which suggest a relationship to boundary
425 layer transport processes. However sediment transport processes also control diversion
426 of river plumes and therefore the location of depocenters, which most likely

427 corresponds to the location of excess pore pressure and gas generation and therefore the
428 most likely location for gravity deformation. In the following sections we review the
429 morphological, seismic, geotechnical and boundary layer processes that, when
430 examined together, allow determining the process at the origin of these features.

431 Assessing the origin of the undulations by sediment creep

432 Influence of gravity-induced sediment instabilities is preferentially invoked in many
433 studies, such as in the Gulf of Castellamare (Agate et al., 2009), the Tiber (Bellotti et
434 al., 1994; Chiocci et al., 1996), Sarno (Sacchi et al., 2005), Fluvià-Muga prodeltas (Díaz
435 and Ercilla, 1993; Ercilla et al., 1995) and early studies of the Adriatic prodeltaic wedge
436 (Correggiari et al., 2001) and the Llobregat prodelta (Checa et al., 1988).

437 In favor of the deformation origin of these structures is that there seems to be a clear
438 spatial relationship between the location of the gas front in the prodeltas and the onset
439 of sediment undulations on most prodelta slopes (Trincardi and Normark, 1988; Urgeles
440 et al., 2008; Cattaneo et al., 2004; Fernández-Salas et al., 2008; Lykousis et al., 2009;
441 Fig. 3, 5 and 6). Gas in shallow water environments is known to affect slope stability in
442 undrained unloading conditions (Vanoudheusden et al., 2004). The lack of a major
443 headwall suggests that in all these areas failure would be at a very incipient stage, if this
444 is the process that actually prevails in these undulated sediment fields.

445 If it is assumed that the sediment undulations are formed by slow gravitational
446 deformation, the lack of compressional features at the toe of the prodelta wedge, as
447 observed in most cases, implies a low angle detachment level. Mud-diapir-like
448 structures have been identified at certain locations of the toe of the Adriatic prodelta
449 wedge (Correggiari et al., 2001), and it could be argued that they result from sediment
450 compression at the toe of the mud-wedge. This genetic association with undulations (as
451 expression of compression at the toe of supposed extension domains represented by the
452 undulations) was proposed by Correggiari et al. (2001) at a time where multibeam
453 bathymetry was not available. However, mud reliefs could also result from fluid
454 expulsion and successive differential deposition guided by the dominant countour-
455 parallel bottom current. In addition to this, there is the fact that such mud reliefs are not
456 found in several other areas of the Adriatic prodeltaic wedge and nowhere else in the
457 fields of undulations of the Mediterranean Sea there are similar features reported (Fig.
458 5).

459 The lack of hyperbolae on the synform part of the folds would also imply that there is
460 no rupture of the reflectors and therefore that deformation is ductile rather than brittle. It
461 is also peculiar that no antithetic shear planes develop in any of the sediment undulation
462 wave fields, while this is a common characteristic of prodeltaic environments where
463 growth faults are present (Bhattacharia and Davis, 2001). Indeed, because within each
464 undulation the dipping of strata is relatively constant as depicted on available seismic
465 reflection data (Ercilla et al., 1995; Chiocci et al., 1996; Correggiari et al., 2001;
466 Cattaneo et al., 2004; Urgeles et al., 2007; Lykousis et al., 2009; Figs. 3, 6, 7 and 8),
467 this implies that there is no synchronous deformation while deposition that could induce
468 growth features (i.e. if the undulations result from sediment deformation there must be
469 one single phase of deformation). In other words, as the deformation is not gradual,
470 creep is not a valid genetic mechanism to explain the sediment undulations.

471 Assessing the origin of the undulations by (partial) slope failure

472 The statements above do not preclude a genesis by sediment deformation, since a
473 genesis due to a punctual event such as an earthquake or major storm is also possible.
474 This event needs to be relatively recent as the undulations affect the whole or the upper
475 Holocene mud wedge in most instances (Figs 3, 6, 7 and 8). Comparing the seismic
476 stratigraphy between adjacent undulations and attempting to trace the reflectors across
477 the supposed shear planes that separate undulations shows that on the upper part of the
478 undulations the displacement is larger than on the lower part (Fig. 6), which is
479 kinematically not possible. Also the fact that the plane separating the different
480 undulations (or angle of climb using sediment bedform terminology) shows no
481 consistent trend with depth, i.e. normally there should be a progressive reduction in
482 angle, appears mechanically incompatible with gravity deformation (Fig. 6). Also the
483 intricate pattern of branching and truncated undulations is common to almost all fields
484 where swath mapping is available (Cattaneo et al., 2003; Urgeles et al., 2007; Fernández
485 Salas et al., 2007; Bárcenas et al., 2009; Figs. 2-3), and this pattern is difficult to explain
486 by gravitational downslope movement, while it is relatively common in sediment
487 transport structures (Mazumder, 2003).

488 An additional exercise to rule out the genesis of the undulations by sediment
489 deformation is to assume that the difference in elevation from trough to crest on the
490 landward side of the undulations corresponds to the vertical component of the
491 deformation. That elevation may reach values of ~0.5 m. From seismic data it can be

492 seen that the slope angle of the plane that separates the different undulations (supposed
493 shear plane) is up to 20°, while the angle of the supposed detachment level at the base of
494 the undulations is less than 1°. Supposing that failure occurs along these two planes in a
495 circular fashion, then the 0.5 m in vertical displacement must translate ~1.5 m
496 horizontal displacement. Because there are various undulations in each sediment
497 undulation field (Ercilla et al., 1995; Chiocci et al., 1996; Correggiari et al., 2001;
498 Cattaneo et al., 2004; Urgeles et al., 2007; Lykousis et al., 2009; Figs. 3, 6-8), this
499 implies that the total horizontal displacement may amount to more than 10 m. Such a
500 large displacement is unlikely to take place without brittle deformation. Thus, the fact
501 that reflectors are not broken is inconsistent with an origin of the undulations by one
502 single phase of sediment gravitational deformation.

503 Finally, Sultan et al. (2008) showed that, at least in the Adriatic case, formation of the
504 undulations by deformation is only possible at a very early stage in the sedimentation of
505 the Holocene mud wedge and that latter undulation evolution or preservation is not
506 related to sediment deformation. Cattaneo et al. (2004) proposed a hybrid genetic
507 mechanism by which the sediment undulations were initiated by seafloor liquefaction,
508 which generated a roughness facilitating the latter growth of the undulations by
509 processes in the bottom boundary layer. As explained earlier, however, most of the
510 undulations root at the MFS (some root at a secondary flooding surface), and such an
511 interpretation would imply that sediment liquefaction occurred shortly after that event
512 took place. Therefore, it is difficult to explain the onset of the many undulation fields in
513 the Mediterranean Sea by generalized liquefaction events at the times when the sealevel
514 attained a relatively high position and spanning passive and active margins. This does
515 not prevent that for some sediment undulation fields some amount of deformation might
516 be involved in the genesis of a seafloor roughness that nucleated the generation of the
517 sediment undulations. Yet, considering the variety of tectonic environments, it is
518 unlikely that the all sediment undulations fields were initiated thanks to sediment
519 deformation induced roughness. Therefore, despite this roughness might be an
520 important factor in the initial development of the sediment undulations, the actual
521 mechanism that generates this roughness, if present at all, does not need to be sediment
522 deformation.

523 Explaining the sediment undulations by processes in the bottom boundary layer

524 All evidence above suggests that the sediment undulations are better explained by
525 bottom boundary layer processes instead of sediment deformation. Amongst the
526 processes acting on Mediterranean prodeltas there are a few of them that could be at the
527 origin of the sediment undulations. We summarize here the various processes that could
528 be at the origin of the sediment undulations and attempt to assign a genetic mechanism
529 to the variety of features observed in the various prodeltaic sediment wave fields (Table
530 2).

531 *Waves and tides*

532 The Mediterranean Sea is a microtidal sea with limited wave period. Only major storms
533 could cause sediment resuspension and transport in water depths below 35 m (see [Puig
534 et al., 2001; Palanques et al., 2002](#)), where most sediment undulations on the prodeltas
535 of the Mediterranean Sea begin to occur (Table 1). Sea waves can only account for the
536 sediment undulations that occur on the shallowest areas of the prodeltas, such as in the
537 Ebro prodelta (Fig. 2B; Table 2). The shallow undulated seafloor features in the Ebro
538 prodelta, located south from the river mouth (Cape Tortosa), seem to be related with
539 enhanced alongshore currents during large wind storms, when near bottom currents in
540 nearby locations can reach 63 cm/s ([Palanques et al., 2002](#)).

541 The effect of waves could barely reach the deepest limit of most sediment undulations
542 fields in the Mediterranean Sea, which is at ~100 m depth such as those of the Tiber,
543 Fluvià-Muga ([Díaz and Ercilla, 1993; Ercilla et al., 1995](#)), Ter ([Díaz and Ercilla, 1993;
544 Ercilla et al., 1995](#)), Llobregat ([Urgeles et al., 2007](#)), Gualdalfeo ([Fernández-Salas et al.,
545 2007; Bárcenas et al., 2009](#)) and also to those that terminate in shallower waters such as
546 that of the Adriatic ([Correggiari et al., 2001; Cattaneo et al., 2004](#)) and many
547 Andalusian prodeltas ([Fernández-Salas et al., 2007; Bárcenas et al., 2009](#)). For example
548 a storm with a return period of 50 years in the Llobregat prodelta area has a significant
549 height and a significant period of 5.1 m and ~10 s respectively ([Bolaños et al., 2001](#)),
550 which would be able to produce water motion at depths down to 86 m. For a 10 year
551 return period storm the significant height and periods are respectively 4.3 m and 9.5 s
552 ([Bolaños et al., 2001](#)), which would be able to produce water motion at depths down to
553 70 m. The storms significant height and period necessary to produce sediment
554 resuspension and mobilization at these water depths is however much higher. It should
555 be noted also that in many areas the sediment undulations are aligned oblique to the

556 direction of wave propagation during major storms, while most bedforms are generally
557 aligned parallel or perpendicular to the predominant currents (Mazumder, 2003).

558 *Hyperpycnal flows*

559 Estimates of solid discharge and sediment concentration in the Mediterranean area can
560 be obtained from rating coefficients (Syvitski et al., 2000). Based on these rating
561 coefficients, historical document sources and paleoflood events determined from
562 slackwater paleoflood deposits, the recorded peak water discharges may induce
563 sediment concentrations high enough to allow the formation of sediment hyperpycnal
564 flows off the Llobregat River (Thorndycraft et al., 2005), off the Po River and a few
565 Apennine rivers (Milliman and Syvitski, 1992; Syvitski and Kettner, 2007) and also off
566 some of the rivers and ramblas of Mediterranean Andalusia (Liquete et al., 2005; Benito
567 et al., 2008). In fact, the Mediterranean rivers of Andalusia are the prototype river that is
568 able to produce hyperpycnal plumes: typically drain small mountainous watershed with
569 easily-erodible sediments, and have low to moderate annual discharge (Imran and
570 Syvitski, 2000).

571 In some prodelta environments there are a number of features that would point to an
572 origin by hyperpycnal flows. For instance, in the Verde and Seco prodeltas the
573 undulations appear to occur on the flank of a prodelta channel which would suggest a
574 relation to hyperpycnal flows spilling over that channel. Also the aspect ratio (L/H)
575 appears to decrease away from the axis of influence of the fluvial inputs (Bárcenas et
576 al., 2009). In the Po River prodeltaic wedge the area displaying undulated sediments
577 occurs where flood deposits have recently accumulated (Wheatcroft et al., 2006)
578 suggesting also a relationship to hyperpycnal flows.

579 In the Andalusian prodeltas a relationship between the aspect ratio (L/H) of the
580 sediment undulations and the discharge characteristics (torrential vs. more fluvial) and
581 slope of the nearby river was also found (Fernández-Salas, 2007; Bárcenas et al., 2009),
582 suggesting that the undulations that have the larger aspect ratio could be induced by
583 hyperpycnal flows (Table 2; Fig. 3). Andalusian river courses that were artificially
584 diverted with respect to the original river path showed two sediment undulation fields:
585 one facing the old river mouth and another facing the newer one. On these occasions, it
586 was found that the undulations close to the recent sediment source have higher L/H
587 ratios (Bárcenas et al., 2009).

588 Recent dam construction, paving and stepping of the river course as well as growth of
589 urban areas in many of the Mediterranean watersheds prevents most sediment to reach
590 the prodelta slope nowadays, and this could be at the origin of the difference in
591 sediment undulation characteristics in prodeltas with an old and a recent sediment
592 source. The facts reported here suggest that hyperpycnal flows could be at the origin of
593 the sediment undulations, at least for the undulations displaying the lower L/H ratios
594 (Table 2; Fig. 3). In many other instances, due to river regulation and climatic forcing,
595 water and sediment discharge have decreased to a point (Ludwig et al., 2009) that
596 prevents hyperpycnal flows to form, at least often enough so that the shallower
597 sediment undulations are able to cope with the competing effect of sea waves (Fig. 6).
598 Therefore maintenance of the undulations by this mechanism on many Mediterranean
599 prodeltas appears not plausible (Puig et al., 2007). This is specially the case for areas
600 where these undulations are relatively widespread laterally, such as in the Adriatic
601 Holocene mud wedge, because river plumes that could give rise to hyperpycnal flows
602 tend to deposit at a relatively short distance from the river mouth (Wheatcroft and
603 Borgeld, 2000; Wheatcroft et al., 2006).

604 **Hyperpycnal flows commonly/rarely go supercritical (Froude number > 1).** The
605 observed undulations in areas where hyperpycnal flows are likely could therefore
606 correspond to cyclic steps. Cyclic steps are sediment waves generated by supercritical
607 or near supercritical turbidity currents (Kostic and Parker 2006; 2007), and often occur
608 associated to channel-levee systems, either within the channel or overbank deposits
609 (Fildani et al., 2006). Cyclic steps have been characterized as long-wave antidunes that
610 are locked in sequence by hydraulic jumps. Its upstream and downstream end are
611 characterized by a short zone over which the flow makes a rapid conversion from
612 shallow, swift supercritical flow ($Fr > 1$) to deep, tranquil sub-critical flow ($Fr < 1$).
613 This locking by hydraulic jumps allows for orderly updip migration. Different flow
614 regimes result in different wavelength of the steps (Fildani et al., 2006). Cyclic steps can
615 be net-erosional and/or net depositional, covering a large spectrum of flow conditions
616 (Fildani et al., 2006; Heino and Davies, 2009). It must be noted however that much
617 smaller wavelength, at least one order of magnitude (20-300 m vs. 1-6 km), is observed
618 in sediment undulations of Mediterranean prodeltas (Table 1) when compared to the
619 ones occurring in deep-water settings (Nakajima and Satoh, 2001, Fildani et al., 2006).
620 A few prototype examples of cyclic steps have however been been mapped and

621 observed to migrate upslope on extremely active shallow prodelta environments (e.g.
622 Hughes-Clarke et al., 2009).

623

624 *Internal waves*

625 Evidence of erosion in the shallowest undulations is present at least on the Llobregat
626 prodelta in relatively shallow waters up to, at least, 30 mbsl (Fig. 6), which suggests that
627 storms have an influence on recent reshaping of the sediment undulation field.
628 However, storms with a recurrence period of 5 years still have a significant wave height
629 and period that is able to produce water motion up to 63 mbsl, and therefore it seems
630 necessary to invoke an additional mechanism for maintaining the sediment undulations
631 on the observed depth ranges (30-90 mbsl). Recent work by Puig et al. (2007) in the
632 Adriatic Sea has shown that internal waves can play a role in resuspending and
633 transporting sediment in prodeltaic undulated areas (Fig. 10). Near-inertial internal
634 waves induced by local wind pulses tend to propagate across the water column through
635 isopycnals and concentrate their energy at the shelf regions where the seasonal
636 thermocline intersects with the seabed, which turns out to be the depth range
637 characterized by having an undulated seafloor (Puig et al., 2007). This is shown in the
638 near-bottom time-series of Fig. 10, which show a remarkable energy peak around 17.7
639 h, mainly in the turbidity and across-shelf velocity spectrum, suggesting that
640 fluctuations induced by near-inertial internal wave activity dominate in the record. Also
641 it is clear in Fig. 10 that near-inertial internal wave activity also contributes to the
642 across-shelf sediment transport in the undulated clinoform region, as turbidity increases
643 associated with this mechanism clearly coincided with periods when the currents were
644 directed offshore and water temperature and salinity decreased. Currents induced by
645 near-inertial internal waves were predominantly directed offshore, while the onshore
646 direction was very weak (Fig. 10). It must be pointed out also that the long crests of the
647 Adriatic undulations, which can be followed for many tens of kilometers in the along-
648 strike direction, parallel to the bathymetric contours (Correggiari et al., 2001; Cattaneo
649 et al., 2004) can only be generated by a process that is continuous and equally intense
650 over a similar distance, as it could occur with internal-waves.

651 Strong near-inertial current fluctuations induced by internal waves have been also
652 observed in other prodeltaic areas of the Mediterranean Sea such as the Ebro prodelta
653 (Puig et al., 2001) and the Llobregat prodelta (Demestre et al., 2004) and they are

654 ubiquitous in the Mediterranean Sea (e.g. Millot and Crépon, 1981; Font et al., 1990;
655 Leder, 2002). In the Central Adriatic, where dedicated experiments were carried out,
656 and also in other prodelta environments (see Table 2) the spatial distribution of seafloor
657 undulations, the decrease of their wavelength and dimensions in the onshore direction
658 and their long, linear crests, suggest that internal waves play a major role in their
659 formation and/or maintenance (see Puig et al., 2007 for a comprehensive discussion).

660 *Bottom currents*

661 In a few cases, the undulations occur in relatively deeper water, are not parallel to the
662 bathymetric contours and have a much larger wavelength (i.e. Fluvià-Muga prodeltas;
663 Table 2; Fig. 2C). On these settings the sediment undulations cannot result neither from
664 hyperpycnal flows nor internal waves and are likely the result from strong bottom
665 currents. In the case of the deeper part of the Fluvià-Muga prodeltas, the origin of such
666 currents appears to be related with the advection of dense shelf waters originated in the
667 Gulf of Lions during storm events, since modeling results reproduce enhanced near
668 bottom currents with high suspended sediment loads over this undulated seafloor region
669 (Ulses et al., 2008, their Fig. 5).

670 Strong shelf currents may also be induced by large wind storms (Bassetti et al., 2006)
671 and/or the general geostrophic circulation (Monaco et al., 1990). For example the
672 “Liguro–Provençal–Catalan Current”, one of the main components of the general
673 circulation in the western Mediterranean, is characterized by speeds ranging from 50 cm
674 s⁻¹ near the surface (Monaco et al., 1990). According to Millot (1990), the core of the
675 Northern Current follows the continental slope most of the time, but the trajectory can
676 be temporally altered during northwesterly wind, when the superficial waters tend to
677 penetrate onto the continental shelf forming a current front that can reach 30 cm s⁻¹ after
678 the wind decay (Millot and Wald, 1980).

679 **Conclusions**

680 a) Sediment undulations are widely present in the Holocene mud wedge of prodeltas
681 in the Mediterranean Sea. Sediment undulations are rooted on a flooding surface,
682 develop within the highstand systems tract and occur in most instances beyond the
683 clinof orm rollover point.

- 684 b) They affect areas of various sizes and, in most instances, have sinuous to rectilinear
685 crests parallel to the bathymetric contours. Wavelength rarely exceeds 400 m and
686 amplitude 5 m.
- 687 c) The geometric characteristics of the plane separating adjacent undulations, the
688 configuration of the reflections down section and between adjacent undulations, the
689 lack of hyperbolae in seismic reflection profiles and the overall morphologic
690 characteristics preclude an origin of the sediment undulations by gravitational
691 instability, either gradual or rapid.
- 692 d) In the Adriatic shelf, sediment deformation has been invoked to explain the initial
693 roughness on which sediment undulations developed as sediment transport
694 structures. In many other areas there is no evidence for such a deformation.
695 Therefore, it is not clear the role of an initial roughness in allowing later
696 development of the sediment undulations. An initial phase of sediment deformation
697 is not a pre-requisite for development of sediment undulations on prodeltaic
698 wedges.
- 699 e) Different processes on the benthic boundary layer might be at the origin of
700 sediment undulations on Mediterranean prodeltas. The most likely mechanisms for
701 the genesis of the sediment undulations are sediment resuspension by internal
702 waves and hyperpycnal flows. Evidence suggests that sediment undulations
703 generated by these two processes probably differ in L/H ratio, with undulations
704 generated by hyperpycnal flows showing lower values. Additional mechanisms that
705 may induce formation of sediment undulations in Mediterranean prodelta settings
706 include waves and derived longshore currents in the shallowest undulation fields, or
707 strong bottom currents in the deepest water sediment undulation fields.

708

709 **Acknowledgements**

710 This manuscript is a contribution to project E-MARSHAL (IGCP-585) funded by IUGS
711 and UNESCO. The data on the Iberian prodeltas was acquired in the frame of the
712 Spanish projects PRODELTA (REN2002-02323) and ESPACE. Thanks are due to the
713 Spanish Institute of Oceanography for access to the ESPACE data. For the Algerian
714 data we thank captain and crew of R/V L'Atalante (campagne PRISME 2007) and
715 funding from French ANR projects ISIS and DANACOR. Borehole geotechnical data
716 was acquired in the frame EC funded project PROMESS-1 (EVR1-CT-2002-40024).

717 Hydrodynamic transects and instrumented moorings were funded by the Office of Naval
718 Research, NICOP Grant N00014-02-1-0252. The “Generalitat de Catalunya” is
719 acknowledged for support through an excellence research group grant (2009-SGR-146).
720 Seismic Microtechnology is acknowledged for Kingdom Suite educational license
721 grant. We thank F. Foglini for figures 3 and 5. J. Déverchère (UBO-IUEM, Brest) and
722 K. Yelles (CRAAG, Algiers) are thanked for discussions about the Algerian shelf.
723 Constructive reviews by XX and XX greatly improved the submitted version of the
724 manuscript.

725 **References**

- 726 Agate, M., Di Grigoli, G., Lo Iacono, C., Lo Presti, V., Mancuso, M., Sulli, A.,
727 Vaccaro, F., 2009. Decoding the instabilities features along the continental margin
728 of sicily (central mediterranean Sea. *Rend. Online Soc. Geol. It.*, 7: 99-101.
- 729 Agate, M., Lucido, M., 1995. Caratteri morfologici e sismostratigrafici della piattaforma
730 continentale della Sicilia Nord-Occidentale: *Naturalista Siciliana*, 29: 3-25.
- 731 Aksu, A.E., Piper, D.J.W., 1983. Progradation of the late Quaternary Gediz delta.
732 *Marine geology*, 54:1-25.
- 733 Albérola, C., Rousseau, S., Millot, C., Astraldi, M., Garcia-Lafuente, J.J., Gasparini,
734 G.P., Send, U., Vangriesheim, A., 1995. Tidal currents in the Western Mediterranean
735 Sea. *Oceanol Acta*, 18: 273-284.
- 736 Balanya, J.C., Garcia-Dueñas, V., Azañon, J.M., 1997. Alternating contractional and
737 extensional events in the Alpujarride nappes of the Alborán Domain (Betics,
738 Gibraltar Arc), *Tectonics*, 16: 226-238.
- 739 Bárcenas, P., Fernández-Salas, L.M., Macías, J., Lobo, F.J., Díaz del Río, V., 2009:
740 Estudio morfométrico comparativo entre las ondulaciones de los prodeltas de los rios
741 de Andalucía Oriental. *Revista de la Sociedad Geológica de España*, 22: 43-56.
- 742 Bard, E., Hamelin, B., Fairbanks, R.G., 1990. U–Th ages obtained by mass
743 spectrometry in corals from Barbados: sea level during the past 130,000 years.
744 *Nature*, 346: 456–458.
- 745 Bassetti, M.A., Jouët, G., Dufois, F., Berné, S., Rabineau, M., Taviani, M., 2006. Sand
746 bodies at the shelf edge in the Gulf of Lions (Western Mediterranean): Deglacial
747 history and modern processes. *Mar. Geol.*, 234, 93-109.

748 Bellotti, P., Chiocci, F.L., Milli, S., Tortora, P., Valeri, P., 1994. Sequence stratigraphy
749 and depositional setting of the Tiber delta: integration of high-resolution seismics,
750 well logs, and archeological data. *J. Sediment. Res.*, 64(3), 416-432.

751 Benito, G., Thorndycraft, V.R., Rico, M., Sánchez-Moya, Y., Sopena, A., 2008.
752 Palaeoflood and floodplain records from Spain: Evidence for long-term climate
753 variability and environmental changes. *Geomorphology*, 101: 68–77.

754 Berné, S., Jouet, G., Bassetti, M.A., Dennielou, B., Taviani, M., 2007. Late Glacial to
755 Preboreal sea-level rise recorded by the Rhône deltaic system (NW Mediterranean).
756 *Marine Geology*, 245: 65-88.

757 Bhattacharya, J.P., Davies, R.K., 2001. Growth faults at the prodelta to delta-front
758 transition, Cretaceous Ferron sandstone, Utah, *Mar. Petrol. Geol.* 18, 525-534.

759 Bolaños R., Jorda, G., Cateura, J., Lopez, J., Puigdefabregas, J., Gomeza, J., Espino, M.,
760 2009. The XIOM: 20 years of a regional coastal observatory in the Spanish Catalan
761 coast. *Journal of Marine Systems*, 77: 237-260.

762 Bornhold, B.D., Prior, D.B., 1990. Morphology and sedimentary processes on the
763 subaqueous Noeick river delta, British Columbia, Canada. In: Colella A., Prior,
764 D.B. (Eds.), *Coarse-grained Deltas*, Spec. Publ. 10. Int. Assoc. of Sedimentol., UK.
765 pp. 169-184.

766 Cacchione, D.A. Drake, D.E. Losada, M.A., Medina, R., 1990. Bottom-boundary layer
767 measurements on the continental shelf off the Ebro River, Spain. *Marine Geology*,
768 95: 179-192.

769 Calvert, A., Sandvol, E., Seber, D., Baranzangi, M., Roecker, S., Mourabit, T., Vidal,
770 F., Alguacil, G., Jabour, N., 2000. Geodynamic evolution of the Lithosphere and
771 upper mantle beneath the Alborán region of the western Mediterranean: Constraints
772 from travel time tomography. *J. Geophys. Res.*, 105: 10871-10898.

773 Cattaneo, A., Correggiari, A., Penitenti, D., Trincardi, F., Marsset, B., 2003.
774 Morphobathymetry of small-scale mud reliefs on the Adriatic shelf. In: Locat, J.,
775 Mienert, J. (Eds.), *Submarine Mass Movements and their Consequences*. Kluwer,
776 Amsterdam, pp. 401–408.

777 Cattaneo, A., Correggiari, A., Marsset, T., Thomas, Y., Marsset, B., Trincardi, F., 2004.
778 Seafloor undulation pattern on the Adriatic shelf and comparison to deep-water
779 sediment waves. *Mar. Geol.* 213 (1–4), 121–148.

780 Cattaneo, A., Trincardi, F., Asioli, A., Correggiari, A., 2007. The Western Adriatic
781 Shelf Cliniform: Energy-limited bottomset. *Continental Shelf Research*, 27: 506-
782 525.

783 Cavaleri, L., 2005. The wind and wave atlas of the Mediterranean Sea - the calibration
784 phase. *Advances in Geosciences*, 2: 255–257.

785 Checa, A., Díaz, J.I., Farrán, M., Maldonado, A., 1988. Sistemas deltaicos holocenos de
786 los ríos Llobregat, Besós y Foix: modelos evolutivos transgresivos. *Acta Geològica*
787 *Hispanica*. 23, 241-255.

788 Chiocci, F.L., Esu, F., Tommasi, P., Chiappa, V., 1996. Stability of the submarine slope
789 of the Tiber River delta. In: Senneset, K. (Ed.), *Landslides*. Balkema, The
790 Netherlands. pp. 521-526.

791 Clark, P.U., Mix, A.C., 2002. Ice sheets and sea level of the Last Glacial Maximum.
792 *Quat. Sci. Rev.* 21: 1–7.

793 Correggiari, A., Trincardi, F., Langone, L., Roveri, M., 2001. Styles of failure in Late
794 Holocene highstand prodelta wedges on the Adriatic shelf. *J. Sediment. Res.* 71,
795 218–236.

796 Demestre, M., Guillén, J., Maynou, F., Palanques, A., Puig, P., Recasens, L., Sánchez,
797 P., Belzunces, M., Bucci, A., Cruz, A., de Juan, S., Visauta, E., 2004. Estimación del
798 impacto de las obras del Plan Director sobre los recursos pesqueros que explota la
799 flota pesquera de la cofradía de Barcelona. Technical report. 302 pp.

800 Díaz, J.I., Ercilla, G., 1993. Holocene depositional history of the Fluviá-Muga prodelta,
801 northwestern Mediterranean Sea. *Marine Geol.*, 111, 83-92.

802 Docherty, C., Banda, E., 1995. Evidence of the eastward migration of the Alborán Sea:
803 A case for basin formation by delamination of the subcrustal lithosphere?. *Tectonics*,
804 14: 804-818.

805 Durrieu de Madron, X., Zervakis, V., Theocharis, A., Georgopoulos, D., 2005.
806 Comments to "Cascades of dense water around the world ocean". *Progress in*
807 *Oceanography*, 64: 83-90.

808 EEA (European Environment Agency), 2006. Waterbase: Transitional, coastal and
809 marine waters (v.4). Available on-line:
810 <http://dataservice.eea.europa.eu/dataservice/metadetails.asp?id=990>.

811 Elgamal, A., Yang, Z. Parra, E., 2002. Computational modeling of cyclic mobility and
812 post-liquefaction site response. *Soil. Dyn. Earthquake Eng.*, 22: 259-271,
813 doi:10.1016/S0267-7261(02)00022-2.

814 England, P., Jackson, J., 1989. Active deformation of the continents. *Ann. Rev. Earth*
815 *Planet. Sci.*, 17: 197-226.

816 Faccenna, C., Piromallo, C., Crespo-Blanc, A., Jolivet, L., Rossetti, F., 2004. Lateral
817 slab deformation and the origin of the Mediterranean arcs. *Tectonics*, 23:
818 doi:10.1029/2002TC001488.

819 Fain, A.M.V., Ogston, A.S, Sternberg, R.W., 2007. Sediment transport event analysis
820 on the western Adriatic continental shelf. *Continental Shelf Research*, 27: 431-451.

821 Fairbanks, R.G., 1989. A 17,000-year glacio-eustatic sea level record: influence of
822 glacial melting rates on the Younger Dryas event and deep-ocean circulation. *Nature*,
823 342: 637–642.

824 FAO (Food and Agriculture Organization of the United Nations), 2007. AQUASTAT:
825 Global River Sediment Yields Database. Land and Water Development Division.
826 <http://www.fao.org/ag/aGL/aglw/aquastat/sediment/index.asp>.

827 Field, M.E., Barber Jr., J.H., 1993. A submarine landslide associated with shallow sea-
828 floor gas and gas-hydrates off northern California. In: Schwab, W.C. et al. (Eds.),
829 *Submarine Landslides: Selected Studies in the U.S. Exclusive Economic Zone*, *Surv.*
830 *Bull. U.S. Geol. Soc.* 2002, USA. pp. 151–157.

831 Fildani, A., Normark, W.R., Kostic, S., and Parker, G., 2006. Channel formation by
832 flow stripping: large-scale scour features along the Monterey East Channel and their
833 relation to sediment waves. *Sedimentology*, 53: 1265-1287.

834 Font, J., Salat, J., Julià, A., 1990. Marine circulation along the Ebro continental margin.
835 *Marine Geology*, 95: 165-177.

836 Gardner, J.V., Prior, D.B., Field, M.E., 1999. Humboldt slide – a large shear-dominated
837 retrogressive slope failure. *Mar. Geol.* 154, 323-338.

838 Galignani, P., 1982. Recent sedimentation processes on the Calabrian continental shelf
839 and slope (Tyrrhenian Sea, Italy). *Oceanologica Acta*, 5: 493-500.

840 Heinio, Davies, 2009. Trails of depressions and sediment waves along submarine
841 channels on the continental margin of Espirito Santo Basin, Brazil, *GSA Bull.*, 121:
842 698-711.

843 Hernández-Molina, F.J., Somoza, L., Rey, J., Pomar, L., 1994. Late Pleistocene-
844 Holocene sediments on the Spanish continental shelves: Model for very high
845 resolution sequence stratigraphy. *Marine Geology*, 120: 129-174.

846 Hill, P.R., Conway, K., Lintern, D.G., Meulé, S., Picard, K., Barrie, J.V., 2008.
847 Sedimentary processes and sediment dispersal in the southern Strait of Georgia, BC,
848 Canada. *Marine Environmental Research*, 66: S39–S48.

849 Hughes Clarke, J.E., Brucker, S., Hill, P. and Conway, K., 2009. Monitoring
850 morphological evolution of fjord deltas in temperate and Arctic regions:
851 International Conference on Seafloor mapping for Geohazard Assessment, Editors:
852 Chiocci F. L., Ridente D., Casalbore D., Bosman A, *Rendiconti online della Società*
853 *Geologica Italiana*, 7 (4):147-150.

854 Imran, J., Syvitski, J.P.M., 2000. Impact of extreme river events on the coastal ocean.
855 *Oceanography*, 13: 85-92.

856 Jiménez, J.A., Guillén, J., Gracia, V., Palanques, A., García, M.A., Sánchez-Arcilla, A.,
857 Puig, P., Puigdefábregas, J., Rodriguez, G., 1999. Water and sediment fluxes on the
858 Ebro delta shoreface. On the role of low frequency currents. *Marine Geology*, 157:
859 219-239.

860 Jiménez-Munt, I., Sabadini, R., Gardi, A., Bianco, G., 2006. Active deformation in the
861 Mediterranean from Gibraltar to Anatolia inferred from numerical modeling and
862 geodetic and seismological data. *J. Geophys. Res.*, 108, doi:10.1029/2001JB001544.

863 Johnson, C., Harbury, N., Hurford, A., 1997. The role of extension in the Miocene
864 denudation of the Nevado-Filabride complex, Betic Cordillera (SE Spain), *Tectonics*,
865 16: 189-204.

866 Jouet, G., Berné, S., Rabineau, M., Bassetti, M.A., Bernier, P., Dennielou, B., 2006.
867 Shoreface migrations at the shelf edge and sea-level changes around the Last Glacial
868 Maximum (Gulf of Lions, NW Mediterranean Sea). *Mar. Geol.* 234: 21–42.

869 Kostic S., Parker G., 2006. The response to a canyon-fan transition: internal hydraulic
870 jumps and depositional signatures. *Journal of Hydraulic Research*, 44: 631-653.

871 Kostic, S., Parke,r G., 2007. Conditions under which a supercritical turbidity current
872 traverses an abrupt transition to vanishing bed slope without a hydraulic jump,
873 *Journal of Fluid Mechanics*, 586: 119-145.

874 Lambeck, K., Bard, E., 2000. Sea-level changes along the French Mediterranean coast
875 for the past 30,000 years. *Earth Planet. Sci. Lett.*, 175: 203–222.

876 Lambeck, K., F. Antonioli, A. Purcell, and S. Silenzi, 2004. Sea level change along the
877 Italian coast from the past 10,000 yr, *Quat. Sci. Rev.*, 23, 1567–1598.

878 Le Vouch, J., Millot, C., Castagné, N., Le Borgne, P., Olry, J.P., 1992. Atlas of
879 Thermal Fronts of the Mediterranean Sea Derived From Satellite Imagery. Mémoires
880 de l'Institut Océanographique, Monaco, 16: 146pp.

881 Leder, N., 2002. Wind-induced internal wave dynamics near the Adriatic shelf break.
882 Continental Shelf Research. 22: 445-463.

883 Lee, H.J., Syvitsky, J.P.M., Parker, G., Orange, D., Locat, J., Hutton, J.H.W., Imran, J.,
884 2002. Distinguishing sediment waves from slope failure deposits: field examples,
885 including the "Humboldt Slide" and modelling results. Mar. Geol., 192: 79-104.

886 Lionello, P., Malanotte-Rizzoli, P., Boscolo, R., Alpert, P., Artale, V., Li, L.,
887 Luterbacher, J., May, W., Trigo, R., Tsimplis, M., Ulbrich, U., Xoplaki, E., 2006.
888 The Mediterranean Climate: An Overview of the Main Characteristics and Issues. In:
889 Mediterranean climate variability, Lionello, P., Malanotte-Rizzoli, P., Boscolo, R.
890 (Eds.), Elsevier, Amsterdam, 421 p.

891 Lionello, P., Sanna, A., 2005. Mediterranean wave climate variability and its links with
892 NAO and Indian Monsoon. Climate Dynamics. 25: 611-623.

893 Liqueste, C., Arnau, P., Canals, M., Colas, S., 2005: Mediterranean river systems of
894 Andalusia, southern Spain, and associated deltas: a source to sink approach. Marine
895 Geology, 222-223: 471-495.

896 Liqueste, C., Canals, M., Lastras, G., Amblas, D., Urgeles, R., De Mol, B., De Batist, M.,
897 Hughes-Clarke, J.E., 2007. Long-term development and current status of the
898 Barcelona continental shelf: A source-to-sink approach, Continental Shelf Research,
899 doi:10.1016/j.csr.2007.02.007.

900 Liqueste, C., Canals, M., Ludwig, W., in prep. Sediment discharge of Mediterranean
901 rivers.

902 Liqueste, C., Canals, M., Ludwig, W., Arnau, P. (2009). Sediment discharge of the rivers
903 of Catalonia, NE Spain, and the influence of human impacts. Journal of Hydrology,
904 366 (1-4): 76-88, doi: 10.1016/j.jhydrol.2008.12.013.

905 Ludwig, W., Dumont, E., Meybeck, M., Heussner, S., 2009. River discharges of water
906 and nutrients to the Mediterranean and Black Sea: Major drivers for ecosystem
907 changes during past and future decades? Progress in Oceanography, 80: 199–217.

908 Lykousis, V., 1991. Submarine slope instabilities in the Hellenic arc region,
909 northeastern Mediterranean Sea. Marine Georesources & Geotechnology, 10: 83-96

910 Lykousis, V., Sakellariou, D., Rousakis, G., 2003. Prodelta slope stability and
911 associated coastal hazards in tectonically active margins: Gulf of Corinth (NE

912 Mediterranean). In: Submarine mass movements and their consequences (Locat, J.,
913 Meinert, J., eds.), 433–440

914 Lykousis, V., Roussakis G., Sakellariou, D., 2009. Slope failures and stability analysis
915 of shallow water prodeltas in the active margins of Western Greece, northeastern
916 Mediterranean Sea. *Int J Earth Sci (Geol Rundsch)*, 98: 807–822

917 Marsset, T., Marsset, B., Thomas, Y., Cochonat, P., Cattaneo, A., Tricardi, F., 2004.
918 Analysis of Holocene sedimentary features on the Adriatic shelf from 3D very high
919 resolution seismic data (Triad survey). *Mar. Geol.* 213 (1–4), 73–89.

920 Martinez-Martinez, J.M., Azañon, J.M., 1997. Mode of extensional tectonics in the
921 southeastern Betics (SE Spain): Implications for the tectonic evolution of the peri-
922 Alborán orogenic system, *Tectonics*, 16: 205-225,

923 Mazumder, R., 2003. Sediment transport, aqueous bedform stability and
924 morphodynamics under unidirectional current: a brief overview. *J. Afr. Earth Sci.* 36,
925 1-14.

926 McKenzie, D.P., 1972. Active tectonics of the Mediterranean region. *Geophys. J. R.*
927 *Astron. Soc.*, 30: 109-185.

928 McKenzie, D.P., 1977. Can Plate Tectonics describe continental deformation?, In *Int.*
929 *Symp. Struct. History Mediterr.* (Biju Duval B., Montadert, L., Eds.), Technip, Paris,
930 189-196.

931 Meybeck, M., Laroche, L., Dürr, H.H., Syvitski, J.P.M., 2003. Global variability of
932 daily total suspended solids and their fluxes in rivers. *Global and Planetary Change*,
933 39: 65-93.

934 Milliman, J.D., Syvitski, J.P.M., 1992. Geomorphic/ tectonic control of sediment
935 discharge to the ocean: The importance of small mountainous rivers. *Journal of*
936 *Geology*, 100: 525-544.

937 Millot, C., 1990. The Gulf of Lions' hydrodynamics. *Cont. Shelf Res.*, 10: 885-894

938 Millot, C., Crépon, M., 1981. Inertial fluctuations on the continental shelf of the Gulf of
939 Lions-Observations and theory. *Journal of Physical Oceanography*, 11: 639-657.

940 Millot, C., Taupier-Letage, I., 2005a. Additional evidence of LIW entrainment across
941 the Algerian Basin by mesoscale eddies and not by a permanent westward-flowing
942 vein. *Prog. Oceanogr.*, 66: 231-250.

943 Millot, C., Taupier-Letage, I., 2005b. Circulation in the Mediterranean Sea. *Env. Chem.*,
944 5: 29-66

945 Millot, C., Wald, L., 1980. The effect of Mistral wind on the Ligurian Current near
946 Provence. *Oceanol. Acta*, 3: 399–402.

947 Monaco, A., Courp, T., Heussner, S., Carbonne, J., Fowler, S.W., Deniaux, B., 1990.
948 Seasonality and composition of particulate fluxes during ECOMARGE-I, western
949 Gulf of Lions. *Cont. Shelf. Res.*, 9–11: 959–987.

950 Mosher, D.C., Thomson, R.E., 2002. The Foreslope Hills: Large-scale, fine-grained
951 sediment waves in the Strait of Georgia, British Columbia. *Mar. Geol.*, 192: 275-295.

952 Mougnot, D., Buillot, G., Rehault, J.P., 1983. Prograding shelf break types on passive
953 margins: some European examples. In: *The Shelfbrak: Critical Interface on*
954 *Continental Margins* (Stanley, D.J., Moore, G.T. eds.). SEPM Special publication,
955 33: 61-77.

956 Nakajima, T., Satoh, M., 2001. The formation of large mudwaves by turbidity currents
957 on the levees of the Toyama deep-sea channel, Japan Sea. *Sedimentology*, 48: 435-
958 463.

959 Niedoroda, A.W., Reed, C.W., Das, H., Fagherazzi, S., Donoghue, J.F., Cattaneo, A.,
960 2005. Analyses of a large-scale depositional clinoformal wedge along the Italian
961 Adriatic coast. *Mar. Geol.* 222–223, 179–192.

962 Normark, W.R., Hess, G.R., Stow, D.A.V., Bow, A.J., 1980. Sediment waves on the
963 Monterey Fan levee: A preliminary physical interpretation. *Mar. Geol.*, 42:, 201-
964 232.

965 Normark, W.R., Piper, D.J.W., Hess, G. R., 1979. Distributary channels, sand lobes, and
966 mesotopography of navy submarine fan, California Borderland, with applications to
967 ancient fan sediments. *Sedimentology*, 26: 749-774.

968 Normark, W.R., Piper, D.J.W., Posamentier, H., Pirmez, C., Migeon, S., 2002.
969 Variability in form and growth of sediment waves on turbidite channel levees. *Mar.*
970 *Geol.*, 192: 23-58.

971 Platt, J.P., Vissers, R.L.M., 1989. Extensional collapse of thickened continental
972 lithosphere: A working hypothesis for the Alborán Sea and Gibraltar arc, *Geology*,
973 17: 540-543.

974 Platt, J.P., Soto, J.I., Whitehouse, M.J., Hurford, A.J., Kelley, S. P., 1998. Thermal
975 evolution, rate of exhumation, and tectonic significance of metamorphic rocks from
976 the floor of the Alborán extensional basin, western Mediterranean, *Tectonics*, 17:
977 671-689.

978 Palanques, A., Durrieu de Madron, X., Puig, P., Fabres, J., Guillén, J., Calafat, A.,
979 Canals, M., Bonnin, J., 2006. Suspended sediment fluxes and transport processes in
980 the Gulf of Lions submarine canyons. The role of storms and dense water cascading.
981 *Mar. Geol.*, 234: 43-61.

982 Palanques, A., Puig, P., Guillén, J., Jiménez, J., Gracia, V., Sánchez-Arcilla, A.,
983 Madsen, O., 2002. Near-bottom suspended sediment fluxes on the microtidal low-
984 energy Ebro continental shelf (NW Mediterranean). *Cont. Shelf Res.* 22, 285-303.

985 Palinkas C.M., Nittrouer C.A., 2006. Clinoform sedimentation along the Apennine
986 shelf, Adriatic Sea. *Marine Geology*, 234: 245-260.

987 Probst, J.L., Amiotte-Suchet, P., 1992. Fluvial suspended sediment transport and
988 mechanical erosion in the Maghreb (North Africa). *Hydrological Sciences Journal*
989 37: 621-637.

990 Puig, P., Ogston, A.S., Guillén, J., Fain, A.M.V., Palanques, A., 2007. Sediment
991 transport processes from the topset to the foreset of a crenulated clinoform (Adriatic
992 Sea). *Continental shelf Research* 27, 452-474.

993 Puig, P., Palanques, A., Guillén, J., 2001. Near-bottom suspended sediment variability
994 caused by storms and near-inertial waves on the Ebro mid continental shelf (NW
995 Mediterranean). *Marine Geology* 178, 81-93.

996 Romagnoli, C., Gabbianelli, G., 1990. Late Quaternary sedimentation and soft sediment
997 deformation features in the Corigliano Basin. North Ionian sea (Mediterranean).
998 *Giornale di Geologia*, 52: 33-53.

999 Rebesco, M., Neagu, R.C., Cuppari, A., Muto, A., Accettella, D., Dominici, R., Cova,
1000 A., Romano, C. Caburlotto, A., 2009. Morphobathymetric analysis and evidence of
1001 submarine mass movements in the western Gulf of Taranto (Calabria margin, Ionian
1002 Sea). *International Journal of Earth Sciences*, 98: 791-805.

1003 RIKZ, IGN, EADS, BRGM, UAB, IFEN, EUCC, 2004. Living with coastal erosion in
1004 Europe: Sediment and Space for Sustainability. EUROSION Atlas Part II: Maps and
1005 statistics. Available on-line: <http://www.euroSION.org/reports-online/part2.pdf>.

1006 Sacchi, M., Insinga, D., Milia, A., Molisso, F., Raspini, A., Torrente, M.M., Conforti,
1007 A., 2005. Stratigraphic signature of the Vesuvius 79 AD event off the Sarno prodelta
1008 system, Naples Bay. *Marine Geol.*, 222-223, 443-469.

1009 Seber, D., Baranzagi, M., Ibenbrahim, A., Demnati, A., 1996. Geophysical evidence for
1010 lithospheric delamination beneath the Alborán Sea and the Rif-Betic mountains.
1011 *Nature*, 379: 785-790.

- 1012 Shackleton, N.J., 1977. The oxygen isotope stratigraphic record of the Late Pleistocene.
1013 Philos. Trans. R. Soc. Lond., B, 280: 169-182.
- 1014 Shackleton, N.J., 2000. The 100,000-year Ice-Age cycle found to lag temperature,
1015 carbon dioxide, and orbital eccentricity. *Science* 289: 1897–1902.
- 1016 Sivan, D., Wdowinski, S., Lambeck, K., Galili, E., Raban A., 2001. Holocene sea-level
1017 changes along the Mediterranean coast of Israel, based on archaeological
1018 observations and numerical model. *Palaeogeography, Palaeoclimatology,*
1019 *Palaeoecology*, 167:101-117
- 1020 Skempton, A.W., 1954. Discussion of the structure of inorganic soils. *J. Soil Mech.*
1021 *Found. Div.*, 80: 263-264.
- 1022 Sultan, N., Cattaneo, A., Urgeles, R., Lee, H., Locat, J., Trincardi, F., Berne, S., Canals,
1023 M., Lafuerza, S., 2008. A geomechanical approach for the genesis of sediment
1024 undulations on the Adriatic shelf, *Geochem. Geophys. Geosyst.*, 9, Q04R03,
1025 doi:10.1029/2007GC001822.
- 1026 Sultan, N., Cochonat, P., Canals, M., Cattaneo, A., Dennielou, B., Haflidason, H.,
1027 Laberg, J.S., Long, D., Mienert, J., Trincardi, F., Urgeles, R., Vorren, T.O., Wilson,
1028 C., 2004. Triggering mechanisms of slope instability processes and sediment failures
1029 on continental margins: a geotechnical approach. *Mar. Geol.* 213 (1–4), 291–321.
- 1030 Syvitsky, J.P.M., Kettner, A.J., 2007. On the flux of water and sediment into the
1031 Northern Adriatic Sea. *Continental Shelf Research*, 27: 296-308.
- 1032 Syvitski, J.P.M., Milliman, J.D., 2007. Geology, Geography, and Humans Battle for
1033 Dominance over the Delivery of Fluvial Sediment to the Coastal Ocean. *Journal of*
1034 *Geology* 115: 1-19.
- 1035 Syvitski, J. P., Morehead, M. D., Bahr, D. B., Mulder, T., 2000. Estimating fluvial
1036 sediment transport: The rating parameters, *Water Resour. Res.*, 36: 2747-2760.
- 1037 Thorndycraft, V.R., Benito, G., Rico, M., Sopena, A., Sánchez-Moya, Y., Casas, A.,
1038 2005. A long-term flood discharge record derived from slack-water flood deposits of
1039 the Llobregat River, NE Spain. *J. Hydrol.* 313, 16-31.
- 1040 Tommasi P., Chiocci F., Esu F., 1998. Geotechnical properties of Soft Clayey
1041 Sediments from the Submerged Tiber River Delta, Italy. *Marine Georesources &*
1042 *Geotechnology*, 16: 221-242.
- 1043 Traykovski, P., Wiberg, P.L., Geyer, W.R., 2007. Observations and modeling of wave-
1044 supported sediment gravity flows on the Po prodelta and comparison to prior
1045 observations from the Eel shelf. *Continental Shelf Research*, 27: 375-399.

1046 Trincardi, F., Cattaneo A., Correggiari, A., 2004. Mediterranean prodelta systems:
1047 natural evolution and human impact investigated by EURODELTA. *Oceanography*,
1048 17: 34–45.

1049 Trincardi, F., Normark, W.R., 1988. Sediment waves on the Tiber pro-delta slope. *Geo-*
1050 *Mar. Lett.* 8, 149-157.

1051 Tsimplis, M.N., Proctor, R., Flather, R.A., 1995. A two-dimensional tidal model for the
1052 Mediterranean Sea. *Journal of Geophysical Research – Oceans*, 100: 16223-16239.

1053 Ulses, C., Estournel, C., Durrieu de Madron, X., Palanques, A., 2008. Suspended
1054 sediment transport in the Gulf of Lions (NW Mediterranean): Impact of extreme
1055 storms and floods. *Continental Shelf Research*, 28: 2048–2070.

1056 UNEP (United Nations Environment Programme), 2003. Riverine transport of water,
1057 sediments and pollutants to the Mediterranean Sea. MAP Technical Reports Series
1058 141, Athens, 111 pp.

1059 Urgeles, R., De Mol, B., Liquele, C., Canals, M., De Batist, M., Hughes-Clarke, J.E.,
1060 Amblàs, D., Arnau, P.A., Calafat, A.M., Casamor, J.L., Centella, V., De Rycker, K.,
1061 Fabrès, J., Frigola, J., Lafuerza, S., Lastras, G., Sánchez, A., Zuñiga, D., Versteeg,
1062 W., Willmott, V., 2007. Sediment undulations on the Llobregat prodelta: Signs of
1063 early slope instability or bottom current activity?. *Journal of Geophysical Research*
1064 112, Art. No. B05102.

1065 Vannucci, G., Pondrelli, S., Argnani, A., Morelli, A., Gasperini, P., Boschi E., 2004. An
1066 atlas of Mediterranean seismicity. *Annals of Geophysics*, 47

1067 Vanoudheusden, E., Sultan, N., Cochonat, P., 2004. Mechanical behaviour of
1068 unsaturated marine sediments: Experimental and theoretical approaches. *Mar. Geol.*,
1069 213: 323-342.

1070 Verdicchio, G., Trincardi, F., 2006. Short-distance variability in slope bed-forms along
1071 the southwestern Adriatic Margin (Central Mediterranean). *Marine Geology*
1072 234:271–292.

1073 Vissers, R.L.M., Platt, J.P., van der Wal, D., 1995. Late orogenic extension of the Betic
1074 Cordillera and the Alborán Domain: A lithospheric view, *Tectonics*, 14: 786-803.

1075 Waelbroeck, C., Labeyrie, L.D., Michel, E., Duplessy, J.-C., McManus, J., Lambeck, K.,
1076 Balbon, E., Labracherie, M., 2002. Sea level and deep water changes derived from
1077 benthic foraminifera isotopic record. *Quat. Sci. Rev.*, 21: 295–305.

- 1078 Wheatcroft, R.A., Borgeld, J.C., 2000. Oceanic flood layers on the northern California
1079 margin: large-scale distribution and small-scale physical properties. *Continental*
1080 *Shelf Research*, 20: 2163--2190.
- 1081 Wheatcroft, R.A., Stevens, A.W., Hunt, L.M., Milligan, T.G., 2006. The large-scale
1082 distribution and internal geometry of the fall 2000 Po River flood deposit: evidence
1083 from digital X-radiography. *Cont. Shelf Res.*, 26: 499-516.
- 1084 Wynn, R. B., Stow, D. A. V., 2002. Classification and characterization of deep-water
1085 sediment waves, *Mar. Geol.*, 192: 7-22.
- 1086

087 Table 1: Morphology and characteristics of major sediment undulation fields in prodeltaic areas of the Mediterranean Sea. \parallel =parallel, \perp =perpendicular, / =oblique, \downarrow =decrease, \uparrow =increase; mwd= meters water depth. Units of
088 length are meters (except otherwise expressed)

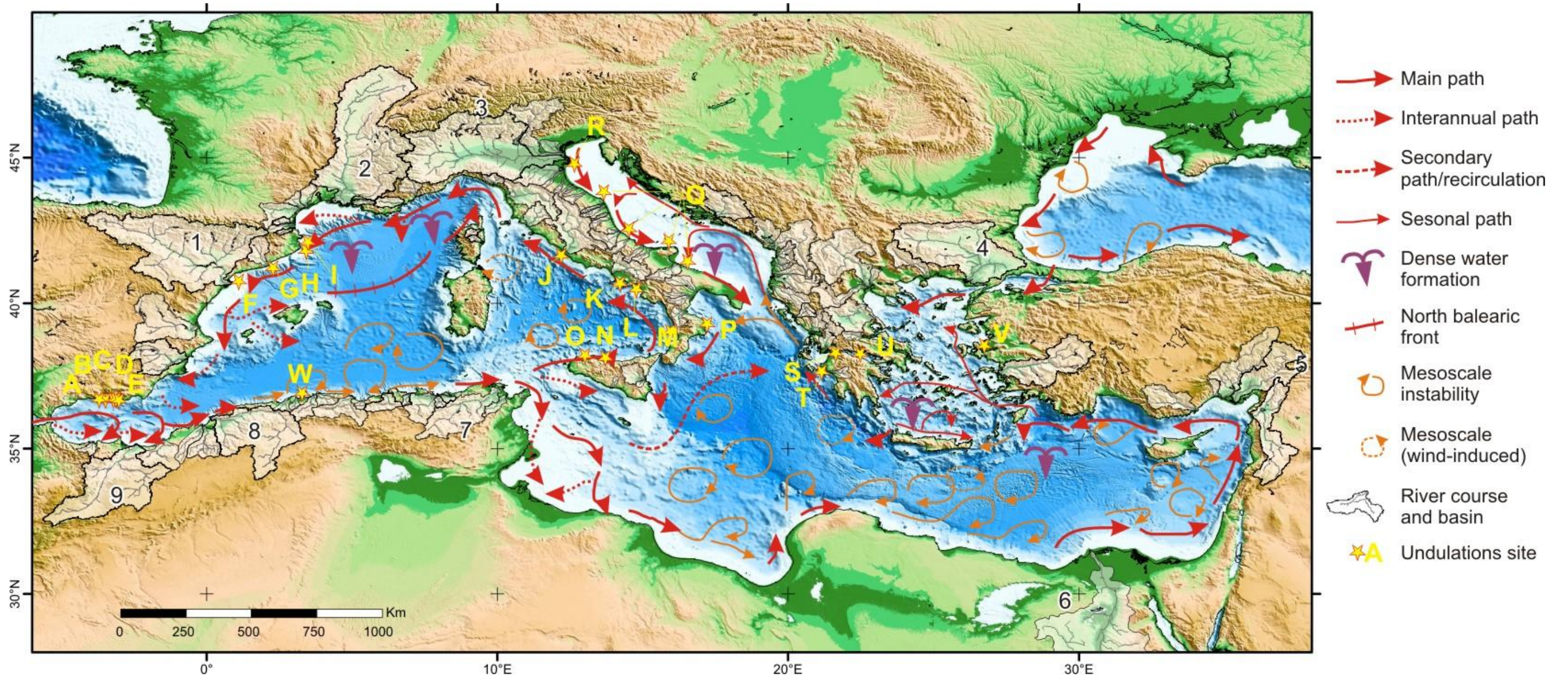
| | Adra | Central Adriatic | Albuñol | Algerian shelf | Ebro | Fluvià-Muga | Guadalfeo | Gualchos | Gulf of Corinth and Kyparissiakos | Llobregat | Seco | Verde | Ter | Tiber |
|--|------------------|--------------------------------|------------------|----------------|---------------|-------------|---------------|------------------|-----------------------------------|--------------------------------|------------------|------------------|-------------|--------------|
| Min. water depth | 18 | 30 | 9 | 55 | 7 | 60 | 10 | 13 | 25 | 35 | 3 | 9 | 60 | 45 |
| Max. water depth | 60 | 70 | 71 | 110 | 15 | 100 | 108 | 56 | 50 | 90 | 65 | 65 | 100 | 100 |
| Wavelength min-max (mean) | 21-244 (76) | 53-477 (212) | 23-163 (61) | | 145-320 (222) | ~1000 | 19-252 (80) | 19-140 (53) | 80-150 | 37-235 (105) | 25-74 (46) | 38-103 (73) | | ~100 |
| Wavelength trend | | \downarrow (> 40 mwd) | | | | | | | | \downarrow | | | | \uparrow |
| Amplitude min-max (mean) | 0.04-2.34 (0.45) | 0.17-3.76 (0.92) | 0.02-4.22 (0.53) | | 0.2-2 (1.1) | 0.5-4 | 0.07-5 (0.85) | 0.02-2.21 (0.32) | | 0.03-1.3 (0.55) | 0.06-2.19 (0.70) | 0.13-1.28 (1.05) | | 7 (max) |
| Amplitude trend | | \downarrow (> 40 mwd) | | | | | | | | \downarrow | | | | \downarrow |
| Sediment type | Gravelly sand | mud | mud | mud | Sand | mud | Silty sand | Silty sand | | Sandy mud | Silty sand | Silty sand | mud | mud |
| Affected thickness | | <35 | | | | 4-25 | | | 10-15 | <30 | | | 5-37 | 30 |
| L/H ratio | ~300 (169) | 100-400 (230) | 296 (115) | | 100-500 (202) | | 129 (84) | ~300 (166) | | 100-400 (191) | 148 (66) | 183 (70) | | |
| Crest length | | | | | 480-1300 | ~100 - 1000 | | | | 300-2000 | | | | |
| Crest pattern | | \approx | | | \approx | | | | | \approx | | | | |
| Crest trend (with respect to bathymetric contours) | \parallel | \parallel | \parallel | | \perp | / | \parallel | \parallel | | \parallel | \parallel | \parallel | \parallel | \parallel |
| Area (km ²) | 6,2 | ~800 | 5,5 | | 3,7 | 20.04 | 25.7 | 3,3 | | 25 | 1,4 | 2 | | 100 |
| Slope | 3.1 | 0.2-1° | 4.5 | | 1° | 0.60 | 2.48 | 3.7 | 0.5-2 | 0.3-3° (2°) | 4 | 5 | 0.75 | 0.7-1.2 |
| Assymetry | ~1.7 | >1 (> 40 mwd) ~1 (< 40 mwd) | 1.6 | | 0.9 | | 1.58 | ~1.2 | >1 | >1 (> XX mwd) ~1 (< XX mwd) | 0.94 | 1.05 | | >1 |
| Sedimentation rates (mm/yr) | | 10 | | | 0.6-3.7 | | | | 3-5 | 0.7-34 | | | | 5.6-28.8 |

1089 Table 2: Distinctive characteristics of the sediment undulation fields with respect to
 1090 assigned genetic mechanism.

| Mechanism at the origin of the sediment undulations | Shape of sediment wave field | Elongation of crests relative to bathymetric contours | Mean L / mean H | Water depth range | Other features | Examples |
|---|--|---|-----------------|-------------------|----------------|--|
| Internal waves | Elongated parallel to shoreline | Parallel | 190-230 | 30-90 | | Central Adriatic, Llobregat, Ter |
| Hyperpycnal flows | Elongated perpendicular to shoreline to circular | Parallel | 60-170 | 3-110 | Channels | Guadafeo, Seco, Verde, Gulachos, Albuñol, Adra, Po |
| Bottom currents | Elongated parallel to shoreline | Oblique to perpendicular | ~450 | 60-100 | | Fluvià-Muga |
| Longshore currents | Circular to parallel to shoreline | Subparallel to perpendicular | ~200 | 3-15 | | Ebro |

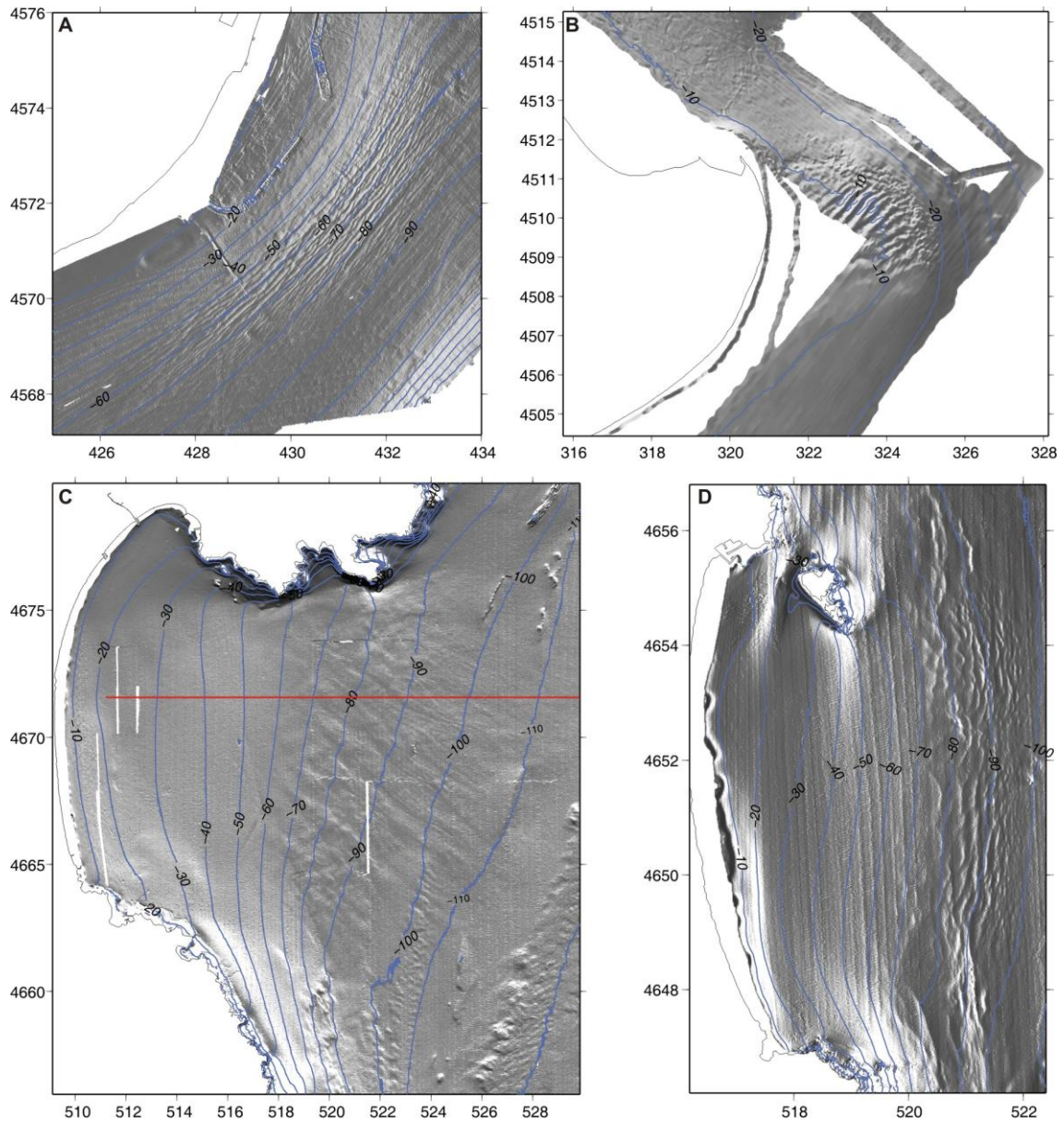
1091

1092

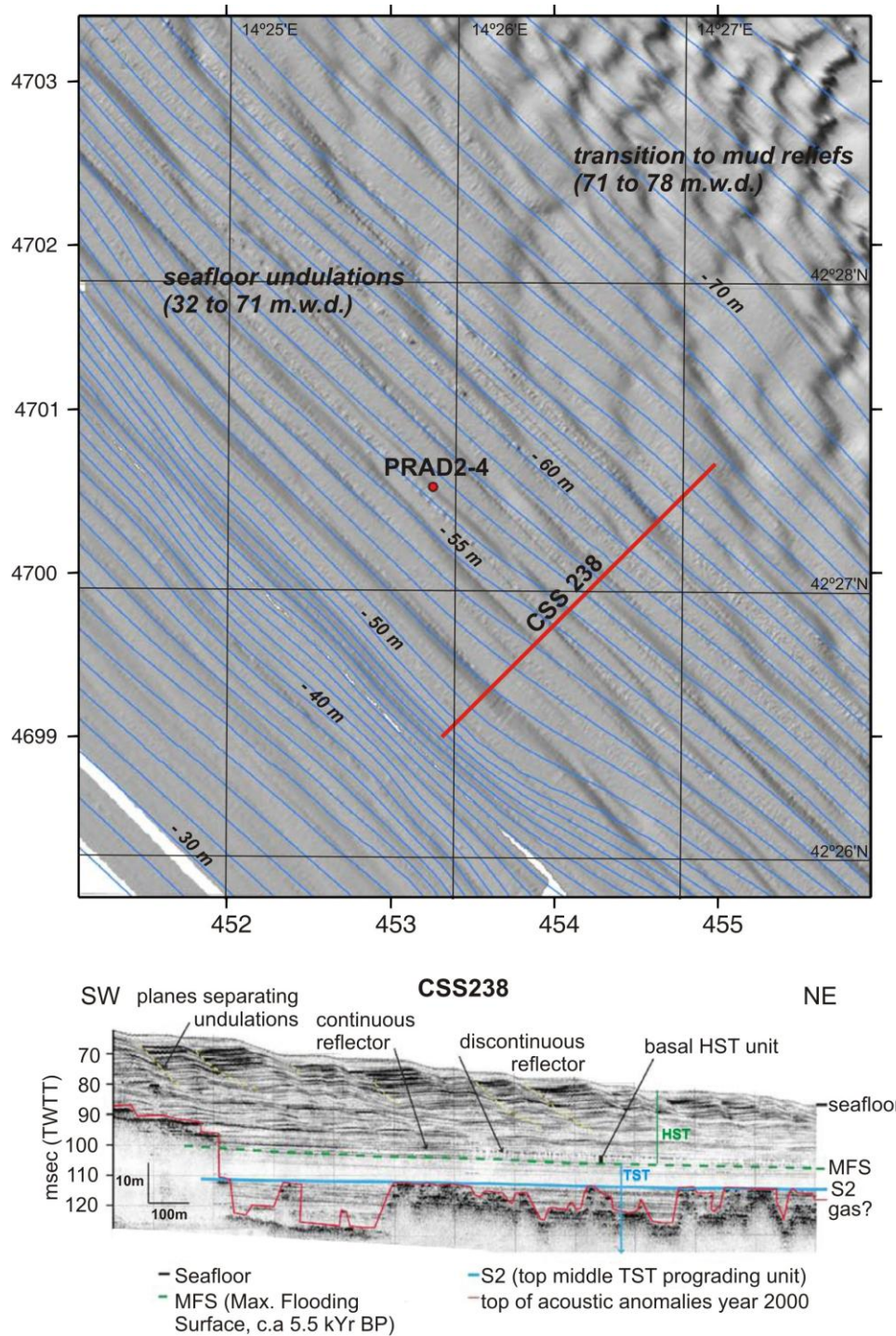


1093

1094 **Fig. 1:** Distribution of undulated sediment features on prodeltas of the Mediterranean Sea (yellow stars) in the frame of surface oceanographic circulation patterns (Millot and Taupier-Letage, 2005b) and major river basins (Liquete et al.,
 1095 in prep.). Major Mediterranean rivers include the Ebro (1), Rhone (2), Po (3), Evros (4), Ceyhan (5), Nile (6), Medjerda (7), Chelif (8) and Moulouya (9). A, Verde and Seco, B, Guadalfeo, C, Gualchos, D, Albuñol, E, Adra prodeltas
 1096 (Fernández-Salas et al., 2007; Bárcenas et al., 2009); F, Ebro prodelta (Urgeles et al., this work); G, Llobregat prodelta (Checa et al., 1988; Urgeles et al., 2007); H, Ter prodelta (Díaz and Ercilla, 1993; Ercilla et al., 1995); I, Furià-Muga
 1097 prodelta (Díaz and Ercilla, 1993; Ercilla et al., 1995); J, Tiber prodelta (Trincardi and Normark, 1988; Chiocci et al., 1996); K, Sarno prodelta (Sacchi et al., 2005); L, Bonea prodelta (Budillon et al., 2005); M, Calabrian shelf (Gallignani
 1098 et al., 1982); N, northern Sicilian shelf (Agate and Lucido, 1995); O, Gulf of Castellammare (Agate et al., 2009); P, Corigliano basin (Romagnoli and Gabbianelli, 1990; Rebesco et al., 2009); Q, Adriatic shelf (Correggiari et al., 2001;
 1099 Cattaneo et al., 2004; Marsset et al., 2004; Berndt et al., 2006; Cattaneo et al., 2007; Puig et al., 2007; Sultan et al., 2008); R, Po prodelta (Correggiari et al., 2001); S, northern Kyparissiakos Gulf (Lykousis et al., 2009); T, Patraikos Gulf
 1100 (Lykousis et al., 1991; Lykousis et al., 2009); U, western Gulf of Corinth (Lykousis et al., 2009); V, Gediz prodelta (Aksu and Piper, 1983); W, Algerian littoral prism (Sultan, unpublished).



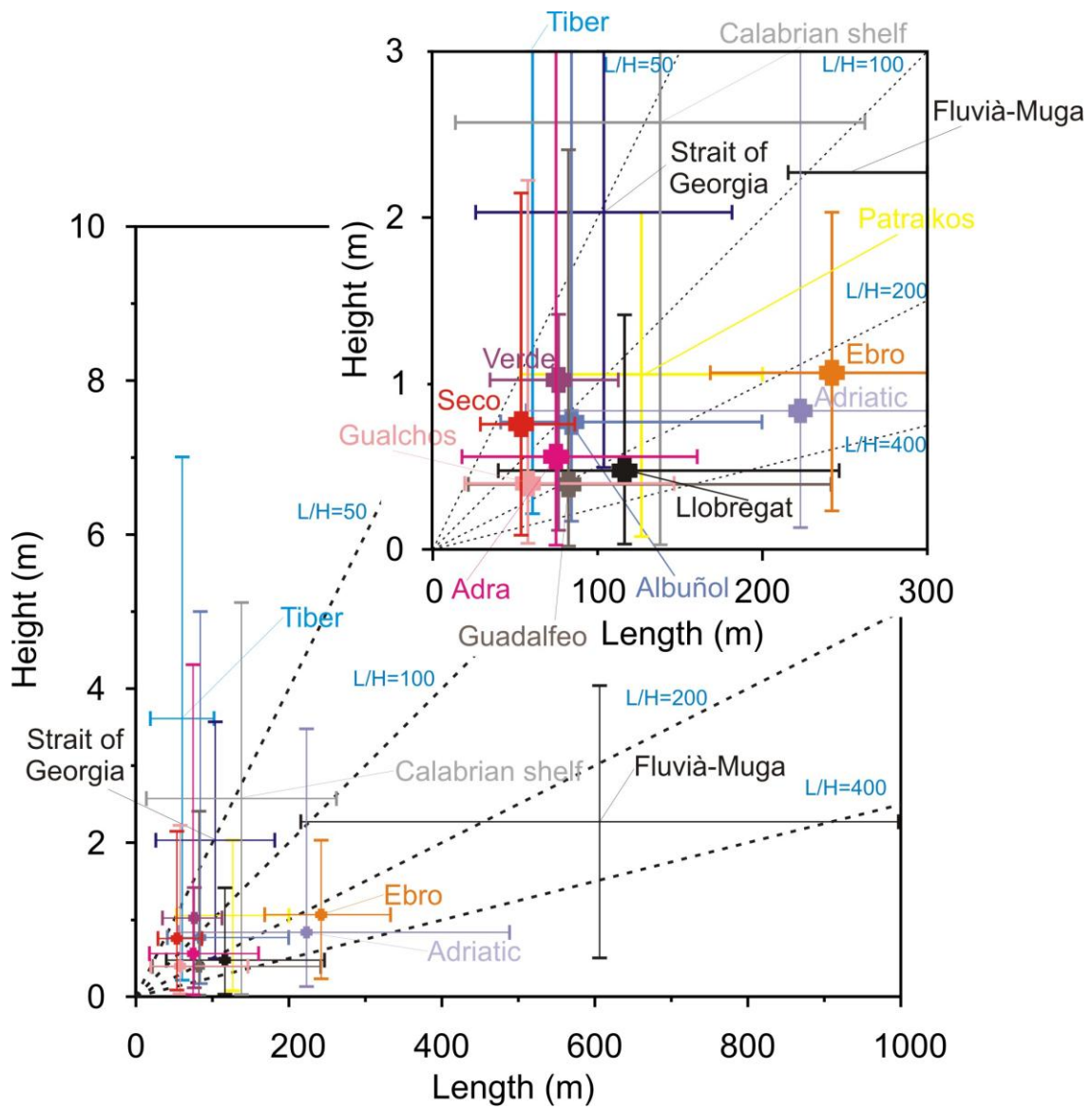
1101
 1102 **Fig. 2:** Shaded relief multibeam maps displaying different types of undulated sediment
 1103 features on prodelta settings. Contours are plotted at 10 m intervals. A) Llobregat
 1104 prodelta, B) Ebro prodelta; C) Fuvià-Muga and D) Ter prodelta. Maps are displayed in
 1105 UTM coordinates for zone 31 (labels in the vertical and horizontal axis display km).
 1106 Red line in C) shows approximate location of Fig. 3B in Ercilla et al., (1995).
 1107



1108

1109 **Fig. 3:** Shaded relief multibeam map on the central Adriatic shelf showing seafloor
 1110 undulations with linear crests aligned in a NW-SE direction, parallel to the coastline,
 1111 between ca. 32 and 71 m of water depth, and a transitional zone to seafloor mud reliefs.
 1112 Map is displayed in UTM coordinates for zone 33 (labels in the vertical and horizontal
 1113 axis display km).. See details in Cattaneo et al., 2004, Fig. 7). The red dot marks the
 1114 location of geotechnical borehole PRAD2-4 (see Sultan et al., 2008 for detail). Red line
 1115 shows location of chirp profile below. See Figs. 1 and 5 for location

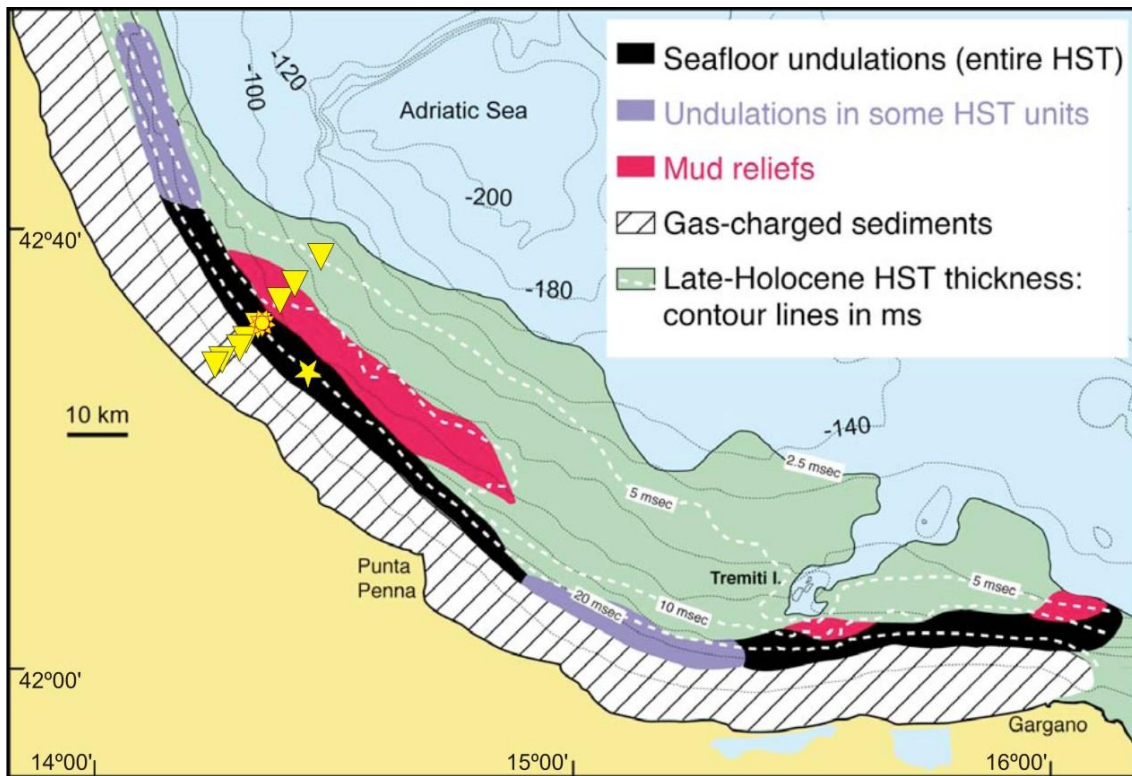
1116



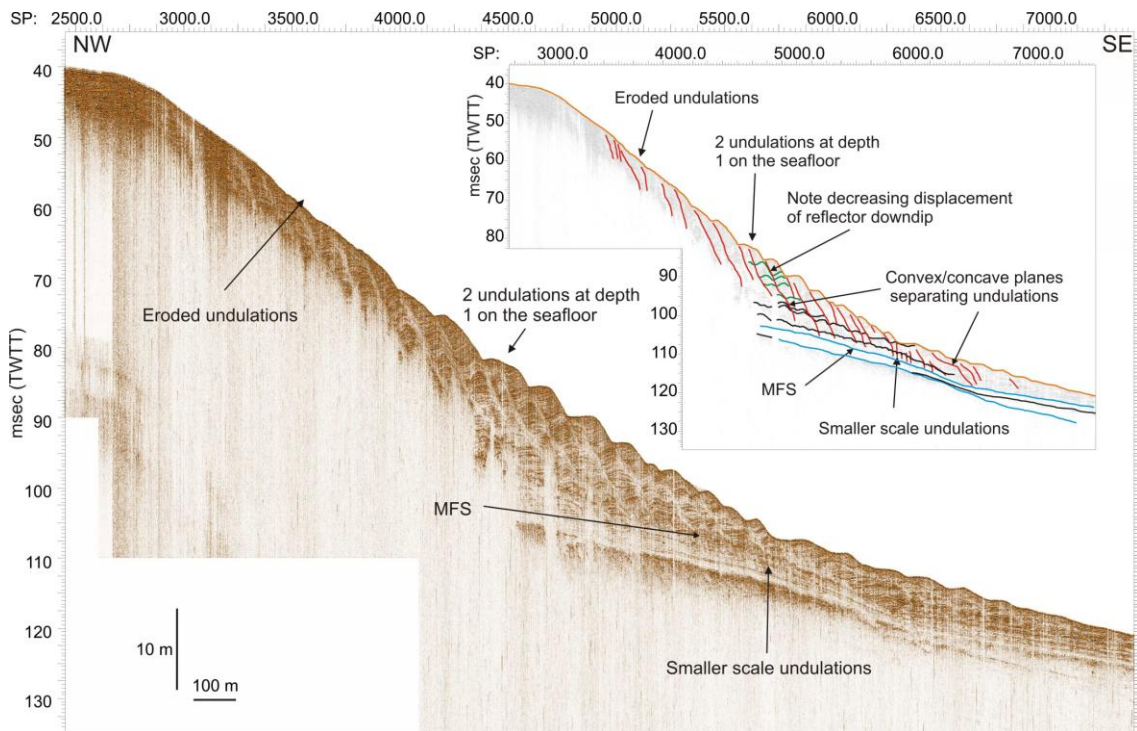
1117

1118 **Fig. 4:** Main morphological features of undulations on Mediterranean prodeltas

1119



1120
 1121 **Fig. 5:** Areal distribution of the sediment undulations and seafloor mud reliefs on the
 1122 central Adriatic shelf. Note that the association between these two features occurs only
 1123 in part of the area with undulations. Modified from Correggiari et al. (2001). Yellow
 1124 star shows location of borehole PRAD2-4. Yellow triangles show CTD stations.
 1125 Complex yellow star with red outline shows location of instrumented mooring.
 1126



1127

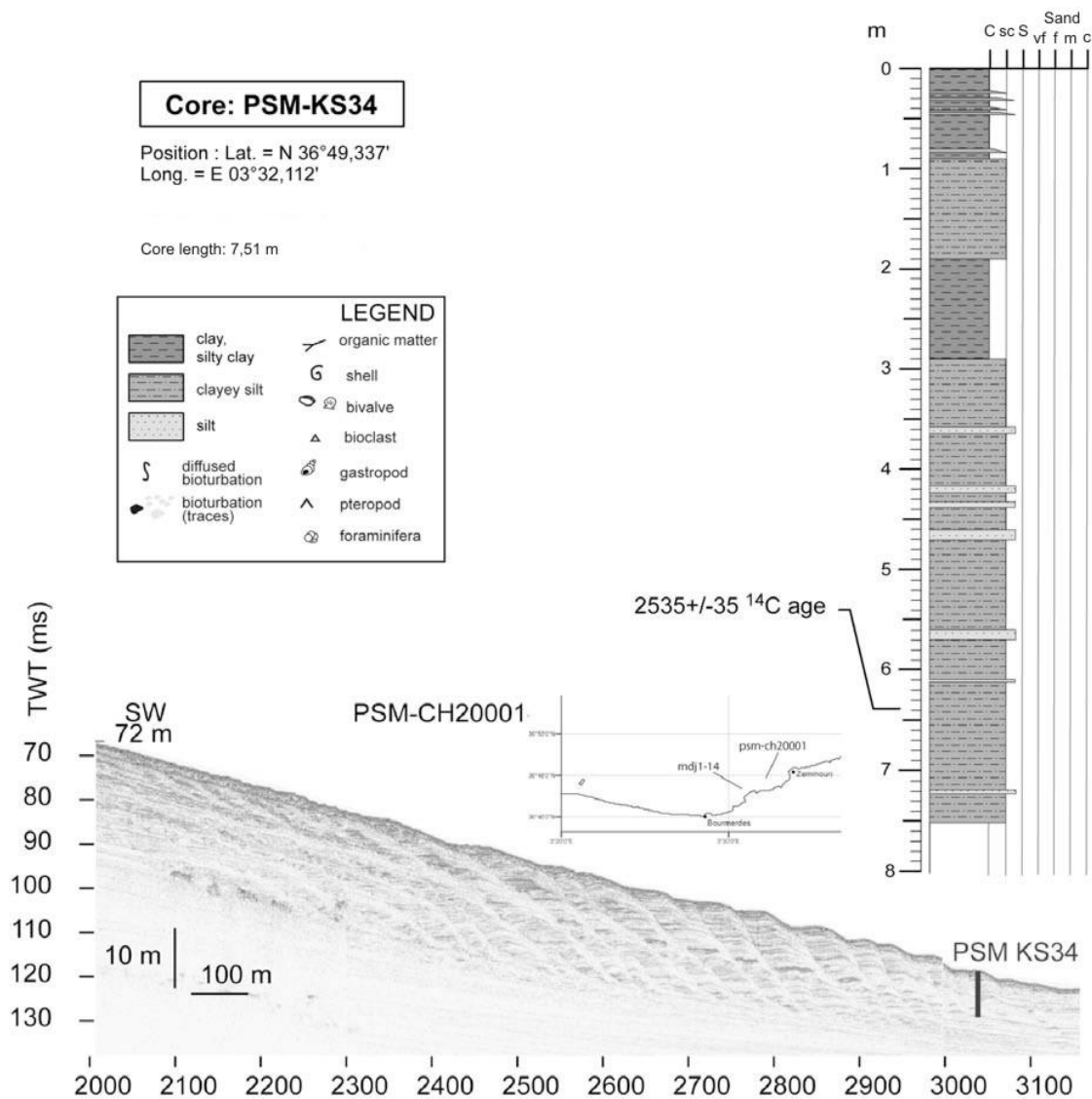
1128 **Fig. 6:** Seismic section showing overall aspect of sediment undulations and internal

1129 structure on the Llobregat prodelta foresets. For location see Fig. 8 (and also Fig. 1).

1130 Inset shows line drawing with the main elements of the sediment undulations that allow

1131 identification as sediment transport structures rather than sediment deformation.

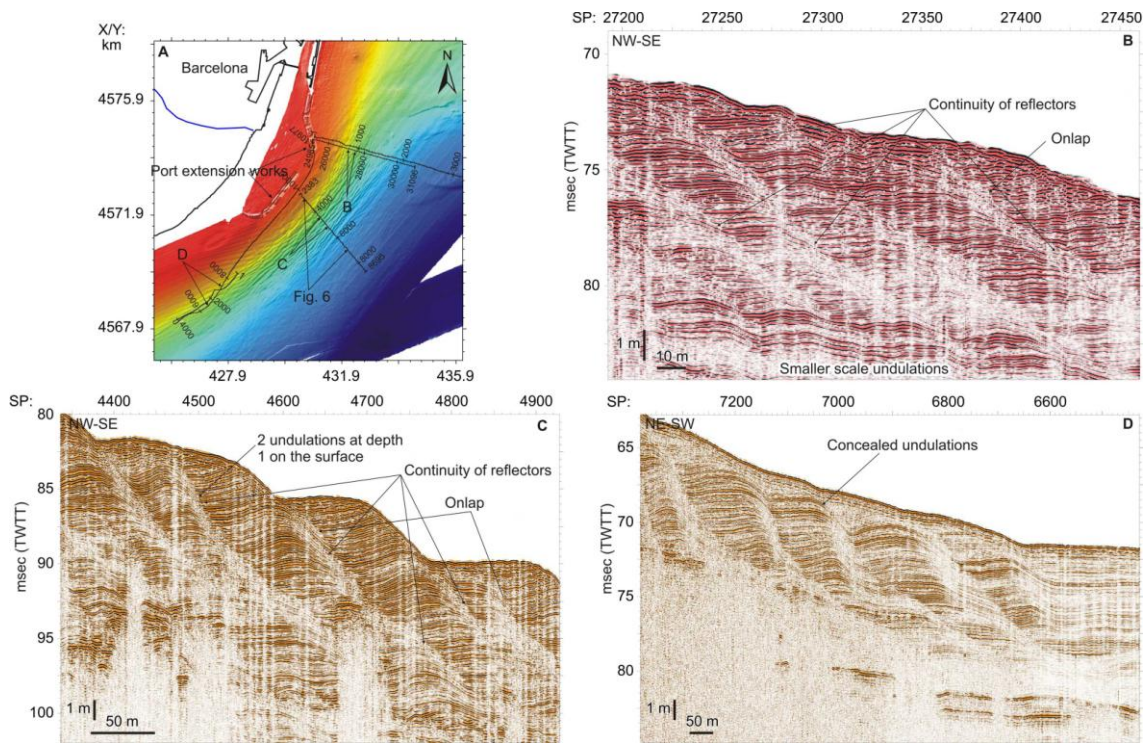
1132



1133

1134 **Fig. 7:** CHIRP-sonar profile on the central Algerian shelf showing sediment
 1135 undulations with a decreasing amplitude and wavelength with increasing depth. The
 1136 sediment core PSM-KS34, at 95 m w.d. recovered a relatively homogeneous succession
 1137 of silty clay. Mixed planktic foraminifera extracted by wet sieving at 6.45 m below the
 1138 seafloor gave a non calibrated age of 2535 +/- 35 kyr BP, confirming that the undulations
 1139 belong to a highstand mud wedge deposited in the late Holocene. See also Fig. 1 for
 1140 location.

1141

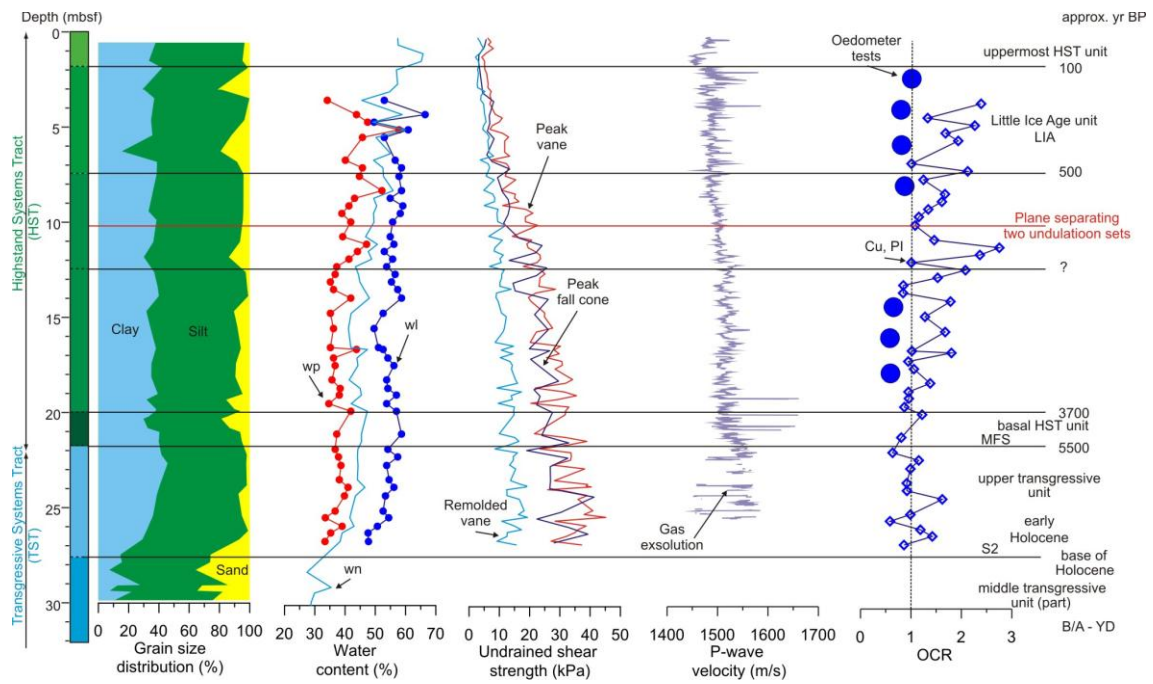


1142

1143 **Fig. 8:** Details of the undulations on the Llobregat prodelta from 5kHz subbottom

1144 profiler data.

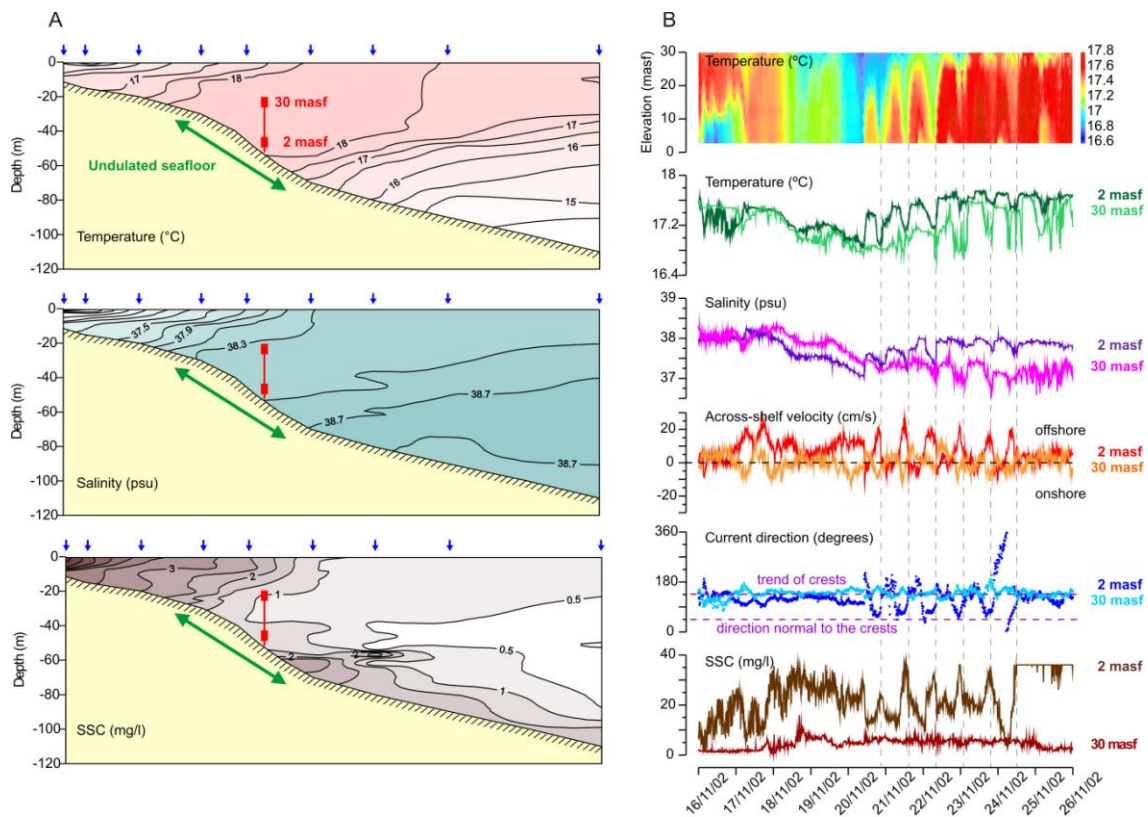
1145



1146

1147 **Fig. 9:** Summary of chrono-stratigraphic and geotechnical characteristics of undulations
 1148 from the Adriatic Sea (wp: plastic limit; wl: liquid limit; wn: natural water content; Cu,
 1149 PI: consolidation state derived from undrained shear strength and plasticity index using
 1150 Skempton's (1954) relationship ($C_u/\sigma'_p=0.0037PI+0.11$); OCR: OverConsolidation
 1151 Ratio). See Fig. 5 for location of Geotechnical borehole.

1152



1153

1154 **Fig. 10:** A. Across-shelf hydrographic sections off Pescara showing the vertical
 1155 distribution of temperature, salinity and SSC recorded on November 2002. Note the
 1156 presence of a surface nepheloid layer, being constrained by coastal colder and less
 1157 saline waters, and the development of a bottom nepheloid layer that detaches where the
 1158 thermocline intersects with the seabed. The location of the instrumented mooring and
 1159 the region affected by an undulated seafloor are also shown. B. Detail of the
 1160 instrumented mooring time series during a period characterized by a strong near-inertial
 1161 signal after the passage of a Sirocco storm. Temperature from 20 to 50 m water depth
 1162 varied with the same periodicity (~17 h) as the fluctuations of the near-bottom turbidity
 1163 and velocity components, indicating a strong displacement of the thermocline and the
 1164 presence of active sediment transport by near-inertial internal waves. Increases of the
 1165 SSC clearly coincide with the offshore direction of the cross-shelf velocity component,
 1166 with current orientations masf normal to the crests of the seafloor undulations. See Fig. 5 for
 1167 location of CTD stations and instrumented mooring.